XMM-Newton

Status of XMM–Newton instrument cross–calibration with SASv10.0

XMM-SOC-CAL-TN-0052 Issue 6.0

M. Stuhlinger, M.J.S. Smith, M. Guainazzi, A. Talavera,
A.M.T. Pollock, R.D. Saxton, M. Santos-Lleo
ESAC, P.O. Box 78, 28691 Villanueva de la Cañada, Madrid, Spain

S. Sembay, A.M. Read
University of Leicester, University Road, Leicester LE1 7RH, United Kingdom

F. Haberl, M.J. Freyberg, K. Dennerl
MPE, Giessenbachstr.1, 85748 Garching, Germany

J. Kaastra, J.W. den Herder, C. de Vries, J. Vink, J. de Plaa
SRON, Sorbonnelaan 2, 3584 CA Utrecht, The Netherlands

XMM–Newton Science Operations Centre

23 December 2010

european space agency
agence spatiale européenne

Issue/Rev.: 6.0
Date: 23 December 2010

XMM Science Operations Team

Page: ii

Contents

XMM Science Operations Team

european space agency
agence spatiale européenne

Issue/Rev.: 6.0

Date: 23 December 2010

XMM Science Operations Team

Page: 1

1   Scope of the document

This document reports the status of the XMM–Newton instrument cross–calibration with SASv10.0 (Science Analysis System) and the public CCFs (Current Calibration Files). The document refers to on-axis observations of various sources. The internal XMM–Newton cross–calibration is analysed, as well as XMM–Newton again Chandra instruments.

More detailed information on the individual instruments are provided in the corresponding calibration status documents which can be found at http://xmm2.esac.esa.int/external/xmm_sw_cal/calib/.

2   Introduction

The European Space Agency's (ESA) X–ray Multi–Mirror Mission (XMM–Newton) was launched by an Ariane 504 on December 10th 1999. XMM–Newton is ESA's second cornerstone of the Horizon 2000 Science Programme. It carries 3 high throughput X–ray telescopes with an unprecedented effective area, and an optical monitor, the first flown on a X–ray observatory. The large collecting area and ability to make long uninterrupted exposures provide highly sensitive observations.

XMM–Newton flies with EPIC and RGS two X–ray instruments built of 5 independent detectors observing simultaneous. Whereas EPIC-pn is using a telescope by its own, two identical copies of RGS and EPIC-MOS at a time share the others.

The XMM–Newton cross–calibration has been under intense investigation during the last few years. Extensive effort has been put into detecting, describing and understanding the calibration differences between the instruments both at ESAC and at the individual PI institutes. This collaboration is still ongoing with regular meetings, also including our colleagues from Chandra, Suzaku, Swift, RXTE and others within the framework of the International Astronomical Consortium for High Energy Calibration (IACHEC [1]) and private communications.

The major breakthroughs in cross-calibration have been:

- **EPIC–pn low-energy response:** In 2005 low-energy refinement of the EPIC–pn response flattened systematic S-shaped residuals.

- **EPIC–MOS patches:** In 2005 the discovery of time and spatially dependent evolution of the EPIC–MOS responses solved the low energy disagreeemnt of EPIC–MOS and EPIC–pn (see EPIC calibration status document, XMM-SOC-CAL-TN-0018, Sect. 1.3.1).

- **EPIC–MOS quantum efficiency:** In 2007 the EPIC–MOS low-energy quantum efficiency was reduced by a maximum of 20% at the O-edge. As a result, EPIC–MOS and EPIC–pn power law spectra agree in spectral slopes and specially the temperatures found in galaxy cluster models agree. But the EPIC–MOS detectors usually return higher normalisations for all energies than the EPIC–pn by about 5-10%.

- **RGS contamination:** In 2006 it was discovered that the RGS sensitivity has been decreasing at wavelengths longer than about 25Å. An empirical effective area correction accounted for this effect (see RGS calibration status document, XMM-SOC-CAL-TN-0030, Sect. 2.1.1). Since 2007 a linear build-up of RGS contamination by pure carbon, probably on the surfaces of the CCDs, is assumed to be the time-variable component to the corrections necessary to deal with a change in the sensitivity at the longest wavelengths.

The most recent improvements to SASv10.0 are described in the following section of this document and are related to EPIC-pn redistribution (Sect. 3.1) and RGS contamination (Sect. 3.2).

Still ongoing topics in the XMM–Newton cross–calibration are the refinement of the time and spatially dependent evolution of the EPIC–MOS responses and the overall normalisation difference between the EPIC–pn and EPIC–MOS.

---

[1]http://www.iachec.org

european space agency
agence spatiale européenne

Issue/Rev.: 6.0
Date: 23 December 2010

XMM Science Operations Team

Page: 2

3 Most recent major changes affecting the cross-calibration

3.1 Adjustment of the EPIC-pn redistribution

The main change in the redistribution matrix of the EPIC-pn camera, released in June 2010 via the calibration file EPN_REDIST_0011.CCF, was a refinement of the energy resolution parameters over the whole energy band. For energies below 2 keV emission line rich spectra, mainly from SNR 1E0102.2-7219 and the star ζ Puppis, were used for the re-calibration. The input spectral models were derived using RGS spectra (see e.g. Plucinsky et al. 2008 for 1E0102.2-7219). For the energies around 6 keV the Mn Kα line produced by the on-board calibration source was used. Due to the slight decrease of charge transfer efficiency with time, the energy resolution was adjusted to yield a zero line width for the beginning of the mission. Further adjustments were done on the redistribution caused by partial events at energies below the O-edge to better fit the low energy N VI and N VII lines of ζ Puppis and to fit the spectrum of the isolated neutron star RX J1856.6-3754 (assuming an absorbed black body spectrum). The redistribution parameters are assumed to be mode independent.

The changes are visualised in Fig. 1 for N VII, O VII, Ne X and Fe-Kα line energies. The dotted line indicates the input energy, the curves represent the EPIC-pn response according to rmf files generated using the corresponding calibration files.
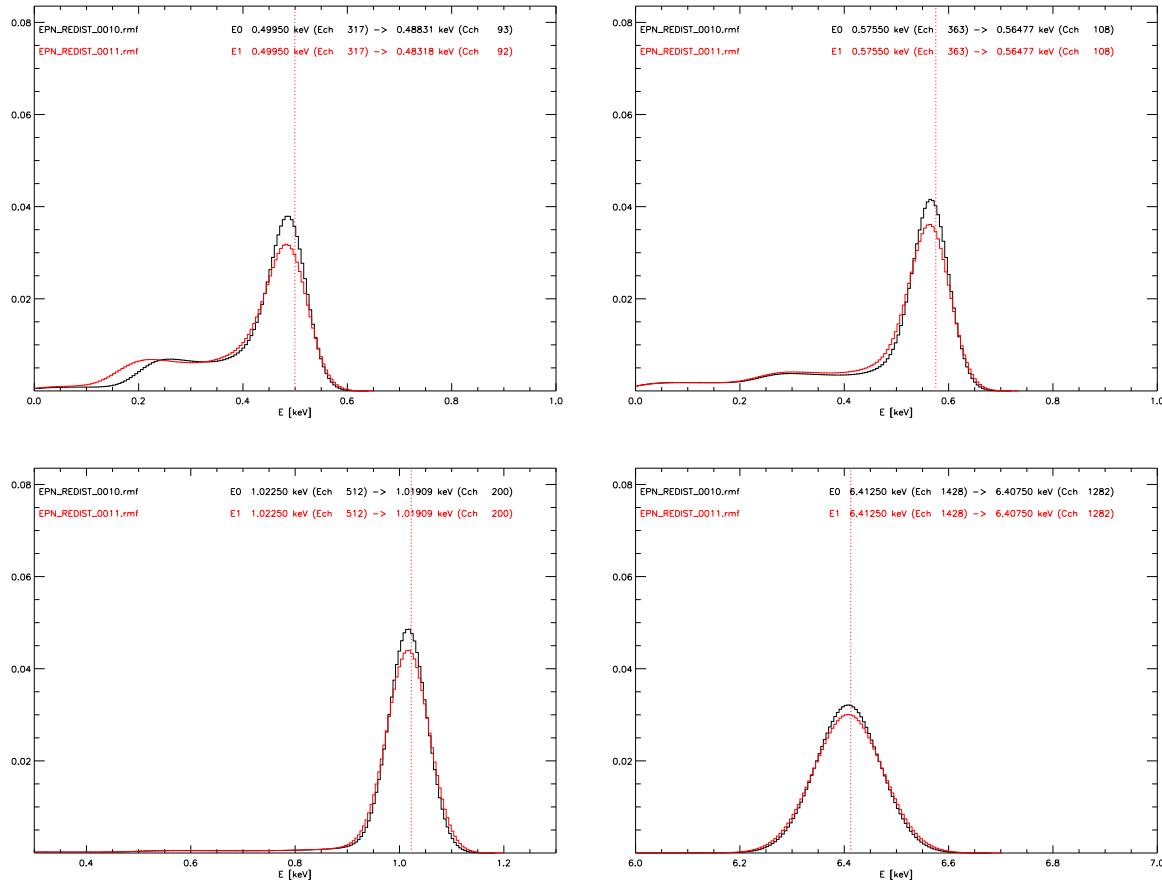

Figure 1: Comparison of the new EPIC-pn redistribution (red: EPN_REDIST_0011.CCF) with the previous version (black: EPN_REDIST_0010.CCF): Stronger redistribution at low energies, in general lower line peaks and slightly reduced line resolution.

european space agency
agence spatiale européenne

Issue/Rev.: 6.0
Date: 23 December 2010

XMM Science Operations Team

Page: 3

3.2 Adjustment of the RGS contamination model

Epoch-dependent empirical RGS effective area corrections were introduced in 2006 based on a set of observations of Mkn421, whose spectrum was assumed to be a simple power-law subject to constant galactic absorption. A year later, it was shown that the time-variable component of the effective area could be modelled by a linearly increasing layer of carbon contamination. Through regular 6-monthly monitoring of RX J1856.6-3754 and the Vela Pulsar Wind Nebula, it has become clear that the build-up of contamination is now slower than the linear model. As shown in Fig. 2, an exponential model gives a good fit. This has been combined with the previous constant polynomial correction to provide a new epoch-dependent correction. The finer temporal resolution requires SASv10.
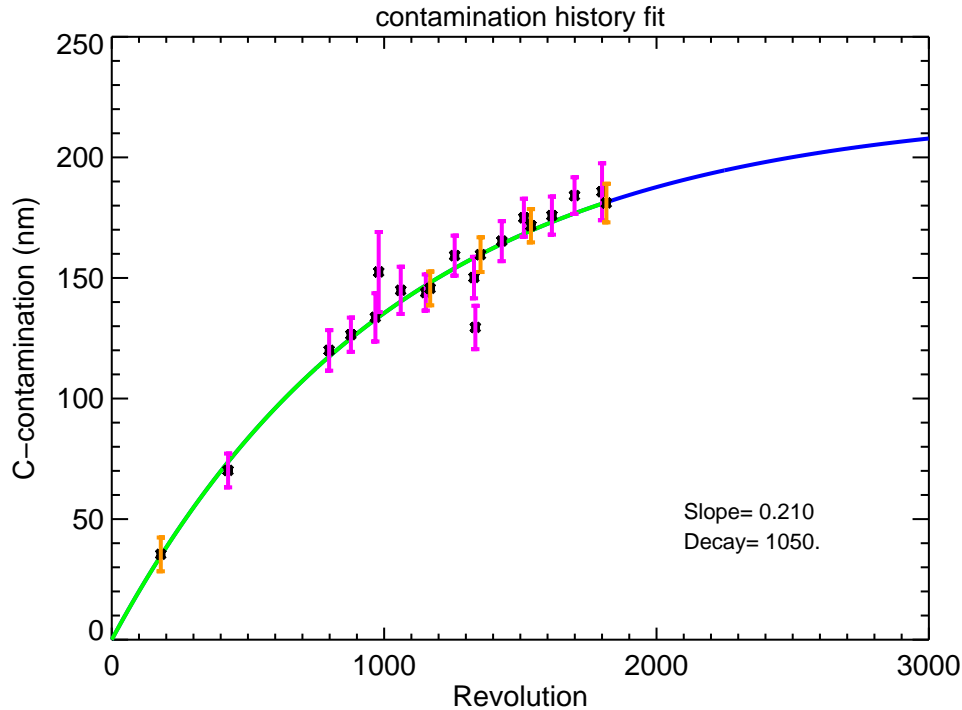

Figure 2: The thickness of the layer of carbon contamination implied by differences in the RGS fluxed spectra of the neutron star RX J1856.6-3754 (pink) and the Vela Pulsar Wind Nebula (orange), both of which are effectively constant. An exponential fit now accounts for the time-variable part of the model of the RGS effective area. Extrapolation into the future is shown by the blue line.

3.3 Consequences of these changes on cross-calibration

The new RGS contamination model leads to lower fluxes at long wavelengths, improving the cross-calibration between RGS and EPIC at low energies (< 0.5 keV). Within the XMM–Newton SOC cross-calibration archive the effect was at about 5%. The effect is larger, $\sim 10\%$ on average, if only observations from mid 2008 onward (rev. ~ 1600) are considered.

The new low energy redistribution of EPIC-pn has significant effects on the cross-calibration between EPIC-pn and RGS, but also between EPIC-pn and EPIC-MOS. The stronger redistribution increases EPIC-pn fluxes at lowest energies by up to 10%. As a result, the combined effect of the new RGS contamination plus the new EPIC-pn redistribution improved the agreement between EPIC-pn and RGS, which in average is now within a few percent. In general, the EPIC-pn and RGS return consistent results for spectral slopes and fluxes. On the other hand, the new EPIC-pn redistribution can cause higher differences between the EPIC-pn and EPIC-MOS instruments at energies below 1 keV.

As an example, Fig. 3 shows a representation of the main differences in cross-calibration from SASv9.0 to SASv10.0.

european space agency
agence spatiale européenne

Issue/Rev.: 6.0
Date: 23 December 2010

XMM Science Operations Team
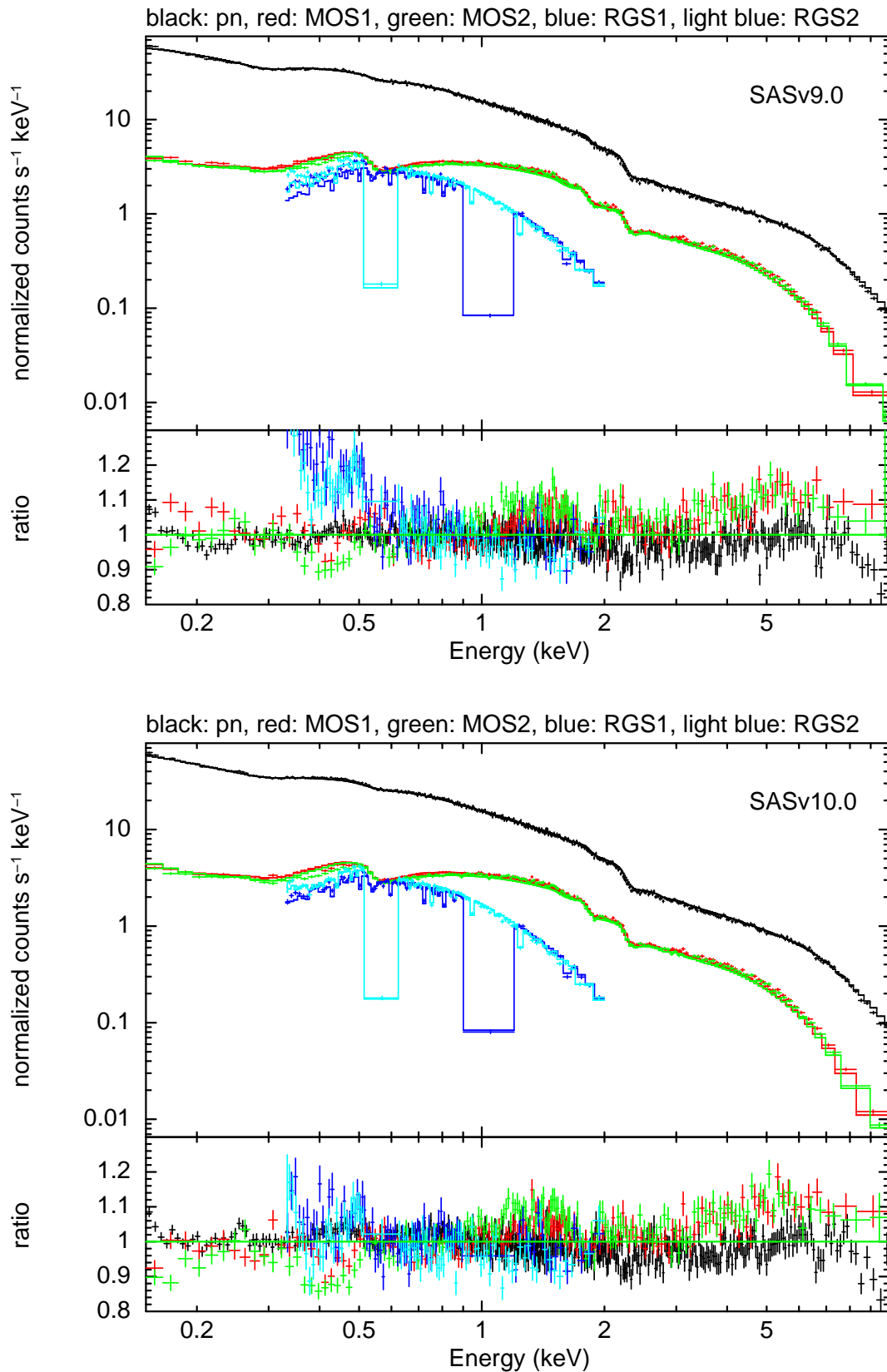
Page: 4

Figure 3: Example of the improvements in XMM–Newton cross–calibration from SASv9.0 (top) to SASv10.0 (bottom). The target is 3C 273 (rev. 1837, ObsID 0414190601) and was fitted with an absorbed double power law model. Using SASv10.0, the RGS and EPIC spectral slopes agree better than in previous versions. In general, EPIC–MOS fluxes are consistently higher than EPIC–pn fluxes.

european space agency
agence spatiale européenne

Issue/Rev.: 6.0
Date: 23 December 2010

XMM Science Operations Team

Page: 5

4 The XMM–Newton SOC cross-calibration archive

4.1 Purpose of the cross-calibration archive

The XMM–Newton SOC cross-calibration archive is designed to enable a fast testing of calibration changes for various sources of different spectral characteristics. Its basis is a software package called XARV which gets the observations from the XMM–Newton science archive, does the data reduction starting from ODF level using a defined calibration version, creates source and background spectra, calculates corresponding response files and performs an automated fitting using XSPEC. Thanks to grid technology impacts of calibration changes can be tested on more than hundred observations of many different sources within a day. Via a web interface, called the *Calibration review tool*, XMM–Newton users worldwide have access to the public part of the cross-calibration archive, presenting results of the official public available calibration versions. Several examples are provided in appendix A.

The Calibration review tool web interface is available at:
http://xmm2.esac.esa.int/external/xmm_sw_cal/calib/cross_cal

4.2 GTI treatment

The cross-calibration archive software first evaluates the GTI times for each X–ray detector individually according to the methods presented in the XMM–Newton SAS Users Guide[2]. Background light curves are created using the selection expressions (`#XMMEA_EP && PI in [10000:12000] && PATTERN==0`) for EPIC-pn and (`#XMMEA_EM && PI>10000 && PATTERN==0`) for EPIC-MOS, respectively. For EPIC-MOS, background rates above 0.35 count/s and for EPIC-pn background rates above 0.4 count/s are excluded. As RGS is less affected by background flares than EPIC, no flare screening is performed for RGS and just the housekeeping GTI for each instrument are taken into account. Finally, the individual GTI files are merged into a single common GTI file, which is used for spectral data extraction of all detectors.

4.3 EPIC pile-up treatment

For EPIC spectra extraction, source and background regions were defined manually for each observations to avoid weak sources within the background region and, for source regions, to exclude pile-up effects in the PSF centres.

To evaluate possible pile-up in EPIC-pn, the single and double events ratios are analysed. In case of pile-up, the single event ratio will decrease in favour of mainly the double event ratio. Using the SAS task `epatplot`, pattern distribution plots are created for a circular source region as well as for annular regions with increasing inner radii. These plots visualise the measured pattern distribution of an observation with the pattern distribution model. Ordered by increasing inner radii, the plot series visualise changes in the pattern distribution and allow the determination of the pile-up free source region, or in other words the radius of the PSF core affected by pile-up.

For EPIC-MOS, the ratio of diagonal to all valid pattern is analysed. Diagonal event patterns can only be created by two individual single events, thus are an indicator for pile-up. PSF core regions with a diagonal pattern fraction of more than about 1% are excluded. This method turned out to be slightly more conservative than the pattern distribution method, which also is applied for EPIC-MOS to confirm the diagonal event analysis.

Finally, the individual EPIC-pn and EPIC-MOS pile-up results are compared for consistency in regard to selected modes and filters.

4.4 Extraction of spectra

The spectral extraction in general follows the procedures provided in the XMM–Newton SAS Users Guide.

The SAS task `rgsproc` already extracts spectra for RGS. The default region setting of `rgsproc` are used, with the source coordinates provided at the `rgsproc`–call and the spectral bins set to wavelength bins

---

[2]XMM–Newton SAS Users Guide: http://xmm.esac.esa.int/external/xmm_user_support/documentation/sas_usg/USG.pdf

european space agency
agence spatiale européenne

Issue/Rev.: 6.0
Date: 23 December 2010

XMM Science Operations Team

Page: 6

(default since SASv10.0). For spectral analyses, only the first order spectra are taken into account.

For EPIC-pn and sources with continuum emission, spectra were extracted using single+double events (`PATTERN in [0:4]`) in combination with `FLAG==0`. For sources with line dominated emission, spectra were extracted using single events only (`PATTERN==0`) in combination with `FLAG==0`. The sources with line dominated emission within the cross-calibration archive are bright, therefore we restrict to single events only which provide the best energy resolution, as the loss of statistics by ignoring split event patterns for these sources is not eminent.

For EPIC-MOS imaging modes and sources with continuum emission, spectra were extracted using single to quadruple events (`PATTERN in [0:12]`) in combination with the predefined flag selection `#XMMEA_EM` and spectral bin size of 15. For sources with line dominated emission, EPIC-MOS spectra were extracted using single events only (`PATTERN==0`) in combination with `FLAG==0`. For these source types the spectral bin size of 5 is used (as of XMM–Newton SAS Users Guide Issue 7.0). For EPIC-MOS timing mode source spectra uses for all source types single events only (`PATTERN==0`) in combination with `FLAG==0`. The corresponding background spectra, taken from peripheral CCDs (imaging mode), in addition to single events, must also include the double events in readout direction (`PATTERN in [0,1,3]`) as well in combination with `FLAG==0`.

4.5 Spectral fitting and flux evaluation

All spectra presented within this document were modelled using XSPEC 12.5.1n, performing χ^2–statistics with "standard" weights. Therefore all spectra are re-binned to get minimum 25 counts per bin and for plot presentation purposes only, the spectra in addition can be re-binned individually using the IPLOT rebin command.

For galactic absorption the abundances of Wilms, Allen & McCray (2000, ApJ 542, 914) were used. For each source, a XSPEC model is defined and the model is used for all observations of the corresponding source. The XARV package does joint fits of all instruments as well as corresponding individual fits for each detector. Fits were performed on the whole available energy range of the corresponding instruments (dependent on modes an count statistics). Using these best fit models, differences between the individual instruments in regard to spectral parameters can be analysed.

Analyses using the whole available energy range makes it difficult to identify the origin of the deviations, and do not allow quantitative deviation measurements within limited narrow energy bands. Also parts of the deviations might be caused by the use of insufficient or even inappropriate spectral models. Therefore in addition a model independent method is required for cross-calibration. Thus, the XARV approximates the measured spectra with a singe power law model within limited narrow energy bands to evaluate bands fluxes and slopes. These energy bands are defined as:

Table 1: Definition of narrow energy bands used in the cross-calibration archive.

Energy band	Lower limit	Upper limit
0.15–0.33 keV	EPIC low energy limit in XARV	RGS low energy limit
0.33–0.54 keV	RGS low energy range limit	Oxygen edge
0.54–0.85 keV	Oxygen edge	Below Neon edge
0.85–2.00 keV	Below Neon edge	RGS upper energy limit
2.00–4.50 keV	RGS upper energy limit	2XMM band
4.50–10.0 keV	2XMM band border	EPIC upper energy limit in XARV

A list of sources which are used for the analysis is provided in Figs. 8+9. All joint fits, corresponding individual fits, the resulting spectral parameters and fluxes in different energy bands of observations presented within this document and various other examples for the cross-calibration status are published on-line via the calibration review tool in the cross-calibration section at the XMM–Newton SOC web page http://xmm2.esac.esa.int/external/xmm_sw_cal/calib.

european space agency
agence spatiale européenne

Issue/Rev.: 6.0
Date: 23 December 2010

XMM Science Operations Team

Page: 7

5 Detector stability: EPIC-pn

In Fig. 4 we show the spectra (*upper panel*) and their residuals against a photoelectrically absorbed black body model (*lower panel*) for the 14 EPIC-pn observations of RXJ1856.6-3754 performed so far. RXJ1856.6-3754 has been routinely observed twice per year since 2002 in the framework of the XMM–Newton Routine Calibration Plan. RXJ1856.6-3754 is one of the seven known candidate isolated neutron stars (INSs) identified in the ROSAT All Sky Survey (Treves et al. 2000, PASP, 112, 297). Their X–ray spectra are extremely soft, and can be generally well modelled with black bodies with temperatures kT=50–100 eV (Burwitz et al. 2001, A&A, 379, L35), although one might expect deviation from a simple black body shape due to atmospheres of either heavy elements (due to debris from the progenitor) or light elements (gravitational setting or accretion; Ho et al. 2007, ApJSS, 308, 279). The soft, stable and featureless X–ray spectrum makes RXJ1856.6-3754 an ideal target for calibration monitoring purposes.

Indeed both the spectra and the residuals in Fig. 4 witness the stability of the response of the EPIC-pn camera along the mission (as well as of the source itself). The overall 0.15–0.85 keV flux (there is flux above this energy) is stable within 1%.
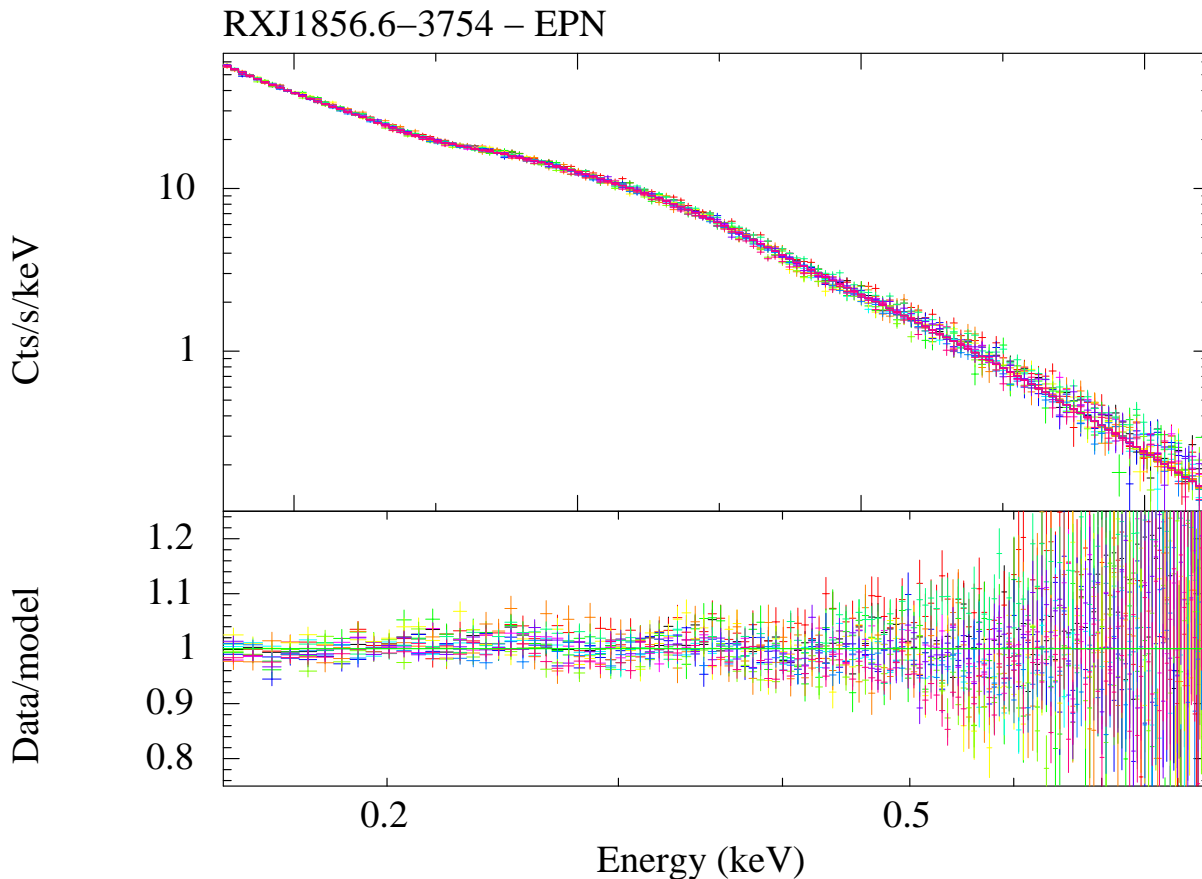
Figure 4: Spectra (*upper panel*) and residuals in units of data/model ratio (*lower panel*) when a photo-electrically absorbed black body model is applied to the EPIC-pn spectra of RXJ1856.6-3754.

Fig. 5 presents the flux in the 0.15–0.85 energy band. In this case a low (at less than 2 σ) variation of the flux is detected: 2.0±1.1%. The 3 σ upper limit is 5%. Considering the individual narrow energy bands 0.15–0.33 keV, 0.33-0.54 keV and 0.54–0.85 keV, there is no evidence for time evolution, it being constrained to be <2.4%, <1.1% and <4.2% in the three bands, respectively (3 σ).

Fig. 6 shows the comparison between the integrated spectra of the "low–temperature" and "high–temperature" states, as defined by the temperature measured in a blackbody fit (threshold: 63 eV) or, equivalently, by the hard X–ray flux. Whether these "states" are due to a calibration issue ot to intrinsic variability of the source has never been clarified, only two observations during the mission are

european space agency
agence spatiale européenne

Issue/Rev.: 6.0
Date: 23 December 2010

XMM Science Operations Team

Page: 8

affected by this hard state). The difference between these two states in the single blackbody scenario is:
$\Delta N_{\rm H} = 8 \pm 3 \times 10^{18}$ cm^{-2}; $\Delta kT = 1.4 \pm 0.2$ eV; $\Delta F = 4.4 \pm 1.3\%$.
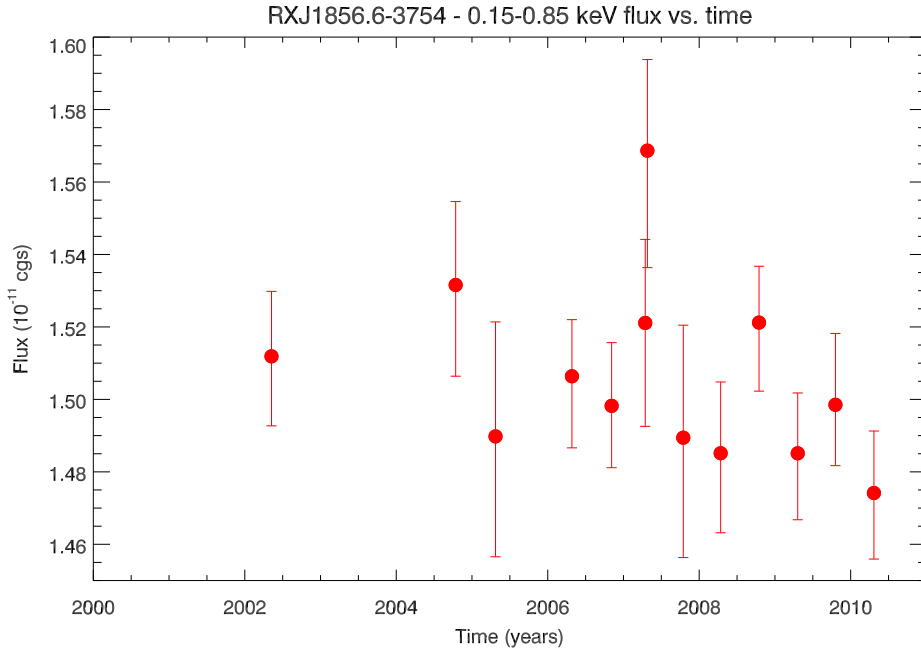

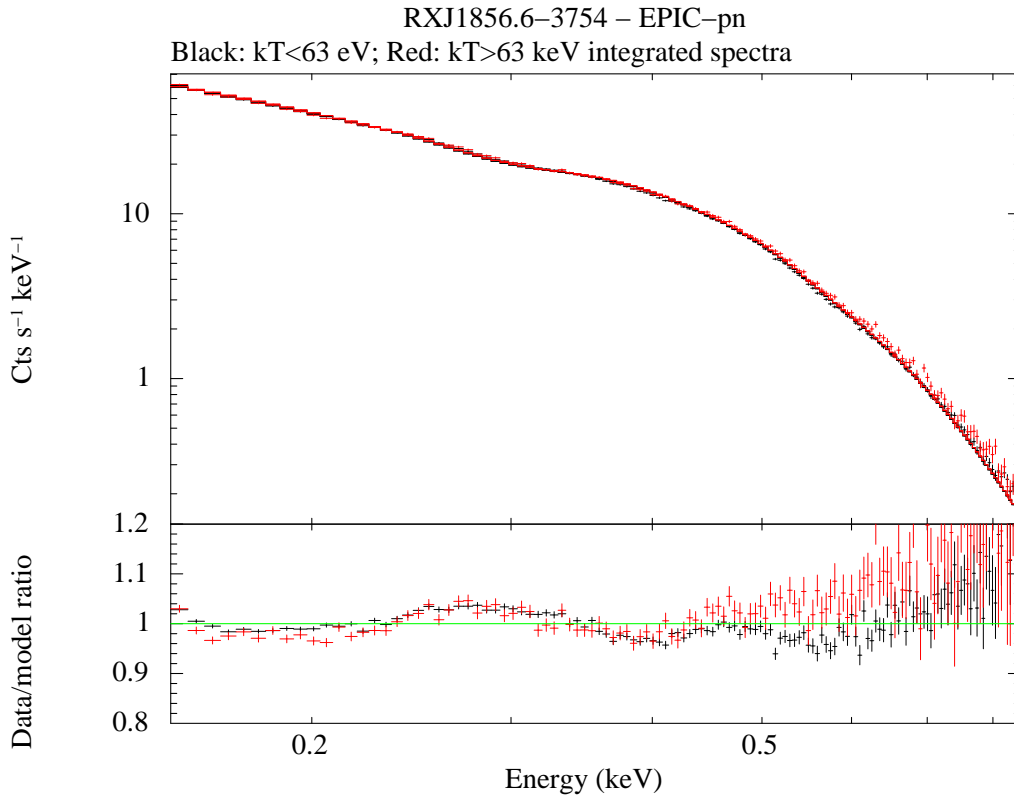Figure 5: Fluxes in the 0.15–0.85 keV energy band for all the RXJ1856.6-3754 observations.

Figure 6: The integrated spectra of the "low–temperature" and "high–temperature" states (threshold: 63 eV).

european space agency
agence spatiale européenne

Issue/Rev.: 6.0
Date: 23 December 2010

XMM Science Operations Team

Page: 9

6 Overall characteristics of XMM–Newton cross-calibration

The cross-calibration archive contains mainly bright sources to obtain high photon statistics. Most of these sources, especially the regularly observated calibration targets 3C 273 and PKS2155-304 are observed in EPIC small window modes and are affected by pile-up. To investigate possible biases on the results due to the source sample selection (bright sources, mainly EPIC small window modes, pile-up), a similar analysis was perfomed on a sample of non-piled-up 2XMM sources observed in EPIC full frame modes. The results of the cross-calibration archive and the 2XMM source sample are consistent. In this section the results of the cross-calibration archive sample is presented, the corresponding 2XMM results are presented in Sect. 7.

The overall XMM–Newton instruments cross-calibration can be investigated by analysing the flux ratios for a high number of sources with different spectral characteristics. All the flux ratios below have been calculated by comparing the fits of individual instruments with the joint fit to all instruments within different energy bands. Due to its higher effective area and high quantum efficiency the EPIC–pn instrument dominates the result of the joint fit. For each energy band, the spectra are approximated with independent single power laws to calculate the fluxes and to evaluate possible systematic slope differences which might not be identified using an appropriate model for a total energy band fit. All results presented in plots of observation samples (Fig. 7–12, 15, 20+21) are based on this method. For this analysis only sources with continuum spectra are used because the used flux evaluation method just described does not provide reasonable results for objects with line-dominated emission.

Next to this narrow band power law approximation method, flux ratios are calculated using individual versus joint best fits for the total energy band and appropriate spectral models for the individual sources. Here, the narrow energy band fluxes were calculated using the individual spectral parameters of the total energy band best fit. This method is not suited to quantify differences in narrow energy bands, as the fit over the total band will average narrow band continuum deviations, but allows the inclusion of emission line sources like stars and supernova remnants for a more general representation of the overall XMM–Newton cross-calibration characteristics. The flux ratio resulting out of these total band spectral model fits are consistent with these of the narrow band power law fits.

The statistics on the flux ratios of various energy bands using more than 100 observations of different types of continuum sources is presented in Fig. 7. At energies above ∼0.8 keV, the EPIC-MOS returns about 5-7% higher fluxes than EPIC-pn. At low energies below ∼0.5 keV, this ratio is inverted, EPIC-pn returns higher fluxes than EPIC-MOS. This result is due to the already public new EPIC-pn redistribution, whereas the corresponding EPIC-MOS updates, due to its complicated spatial and time dependence of the patches, are not yet available.

Below ∼0.5 keV, RGS and EPIC-pn fluxes agree very well. At energies above ∼0.5 keV, RGS returns about 3-4% lower fluxes than EPIC-pn.

Fig. 8 provides the time evolution of the flux ratios and Fig. 9 the corresponding slope differences within the same energy bands over the mission. The target names and the numbers of observations for each object (in brackets) are provided in the plot. It is obvious that the results can be quite variable between one source and another.

The energy bands above 0.85 keV show a nearly stable situation for all the EPIC-instruments, showing no systematic time evolution neither for flux nor slope differences. At lower energies, the data are consistent with no time evolutions after revolution ∼800, but there are differences in the EPIC-MOS to EPIC-pn flux ratios before revolution ∼800 and afterwards.

The RGS does not show systematic time evolutions over the mission.

Examples of joint fits are presented in the appendix using series of two sources, the quasar 3C 273 (Sect. A.1) as a continuum source, and 1E0102.2-7219 (Sect. A.2) as a emission line source. In addition to these, more examples in Sect. A.3–A.7 using various sources at different epochs demonstrate the current status of the EPIC/RGS cross–calibration using SASv10.0. All figures show joint fits for all five X–ray instruments, and thus use the identical set of model parameters without normalisation constants. Details can be found with the calibration review tool at the XMM–Newton SOC web page http://xmm2.esac.esa.int/cgi-bin/ept/preview.pl.

european space agency
agence spatiale européenne

XMM Science Operations Team

Issue/Rev.: 6.0
Date: 23 December 2010

Page: 10
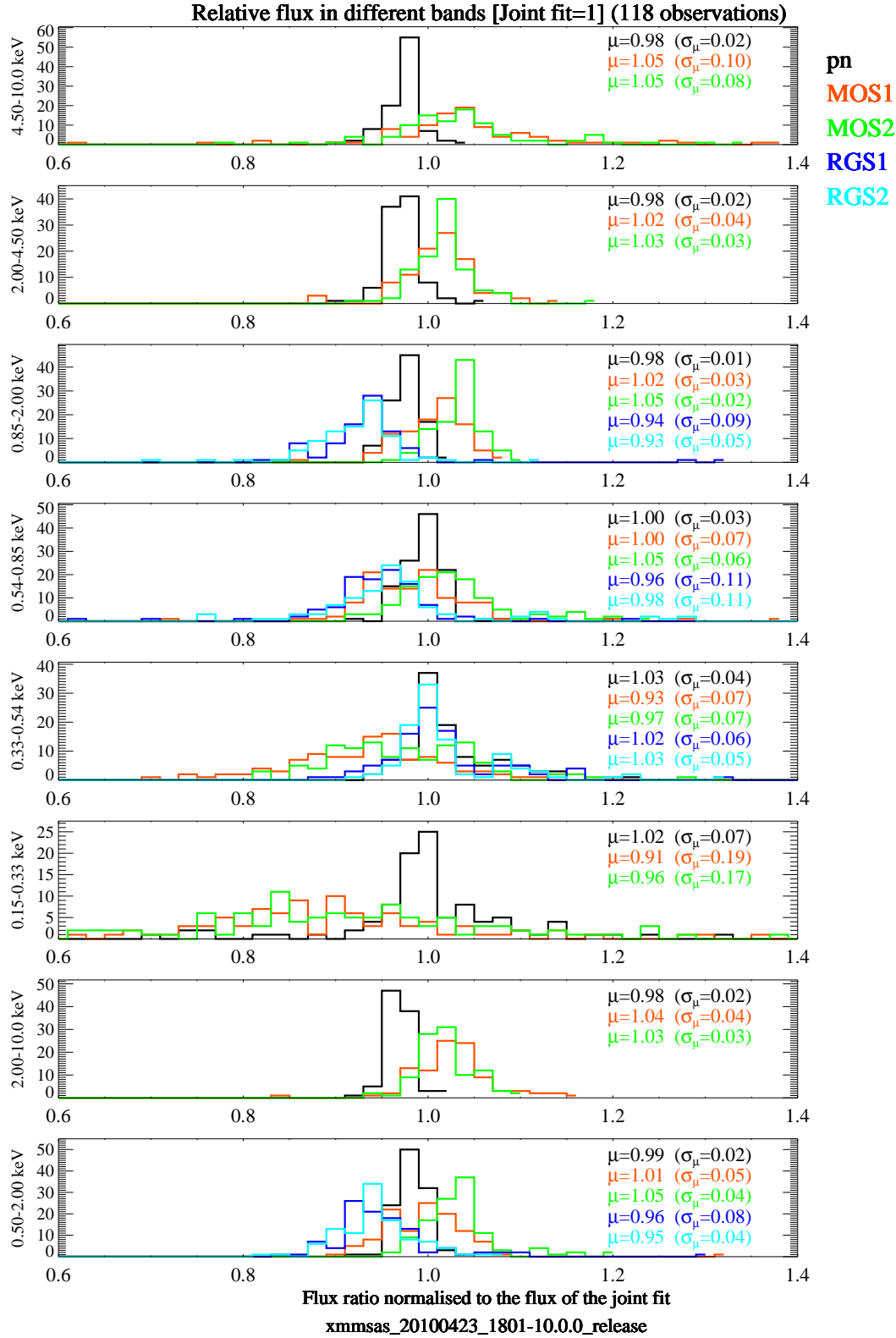
Figure 7: Flux ratios of individual single power law fits to joint fit within six narrow energy bands and two broad energy bands. The numbers provided are the mean of the distributions (μ) and the corresponding standard deviations (σ_μ).

european space agency
agence spatiale européenne

Issue/Rev.: 6.0
Date: 23 December 2010

XMM Science Operations Team

Page: 11

Relative flux ratio history

Symbol	Object			
✳ 3C273 (25)	◇ PKS2155−304 (20)	□ RXJ1856.6−3754 (17)	△ PKS0558−504 (08)
✕ H1426+428 (07)	+ PG1116+215 (06)	+ A2029 (05)	+ Mkn501 (04)
+ APM08279+5255 (04)	+ PKS0548−322 (03)	+ H2356−309 (03)	+ A3112 (03)
+ A262 (03)	+ Mkn180 (02)	+ MS0737.9+7441 (02)	+ 3C120 (02)
+ 3C111 (02)	+ 1H0414+009 (02)	+ PKS2351−154 (01)	+ H1101−232 (01)
+ Ark120 (01)	+ A1795 (01)	+ 1H1219+301 (01)	Total: 123 obs

Figure 8: Flux ratios of individual single power law fits to joint fit within narrow energy bands over time in revolutions, including the targets and the numbers of observations for each object (in brackets).

european space agency
agence spatiale européenne

Issue/Rev.: 6.0
Date: 23 December 2010

XMM Science Operations Team

Page: 12

Relative slope difference history

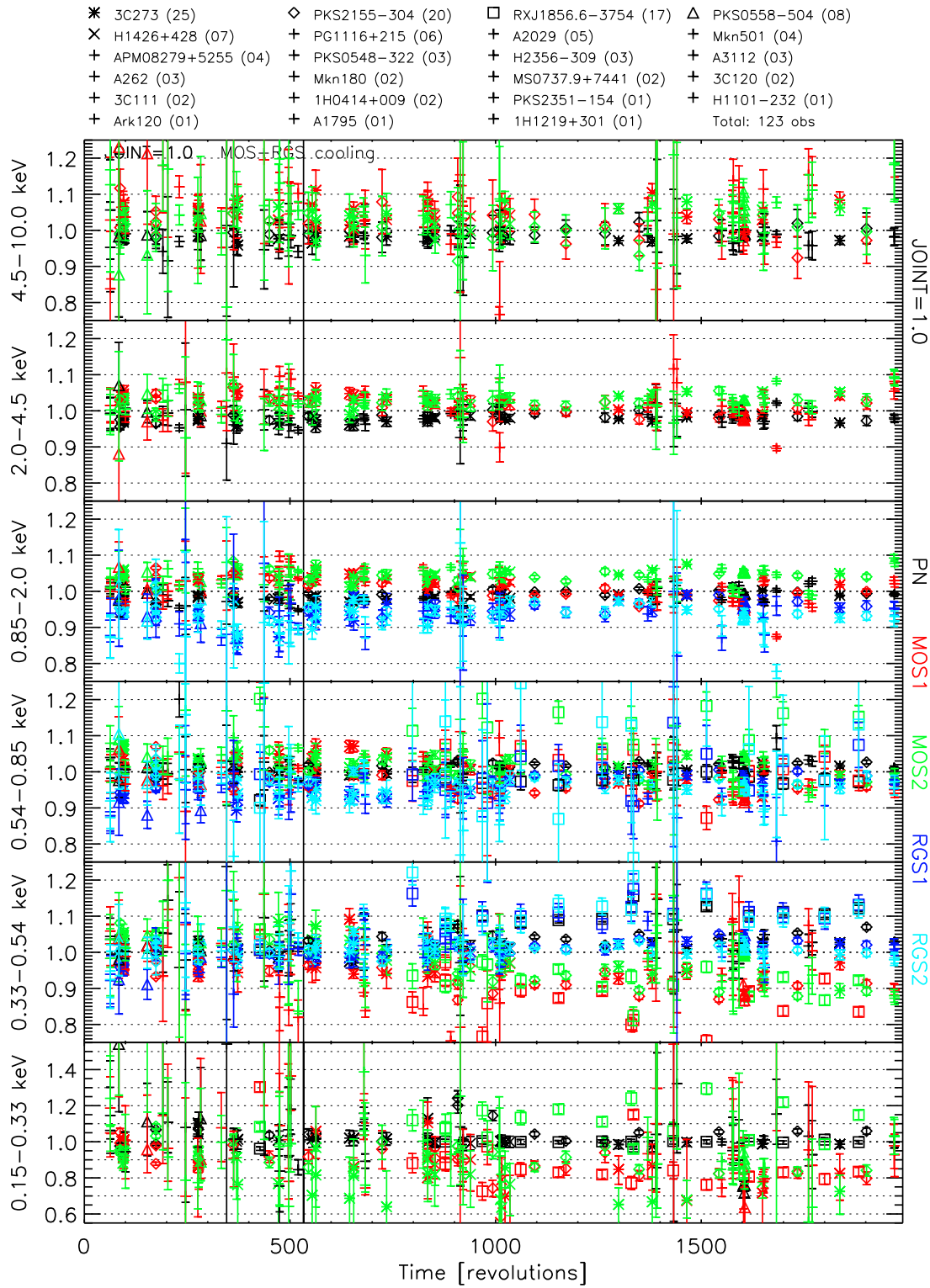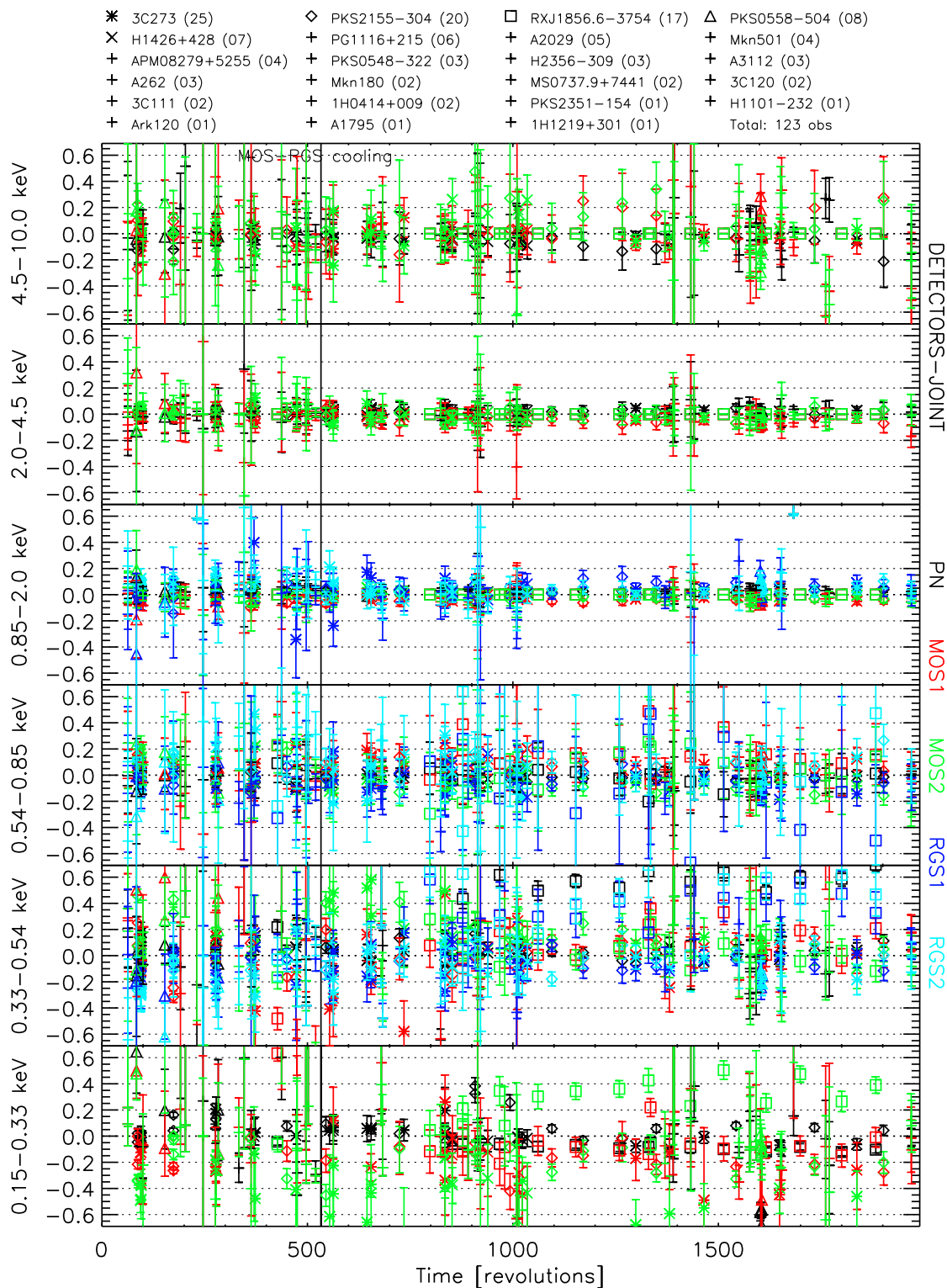Figure 9: Slope differences of individual single power law fits to joint fit within narrow energy bands over time in revolutions, including the targets and the numbers of observations for each object (in brackets).

european space agency
agence spatiale européenne

Issue/Rev.: 6.0
Date: 23 December 2010

XMM Science Operations Team

Page: 13

7   EPIC cross-calibration with 2XMM

In this Section we investigate the quality of the EPIC cross-calibration using a large sample of on-axis sources extracted from the 2XMM catalogue of EPIC serendipitous sources (Watson et al. 2009, A&A, 493, 339). As of January 2010, 2XMM contains more than 200,000 unique sources. We stress that using the study discussed in this Section is not a mere repetition of the XCAL. Most of the XCAL sources are comparatively bright and therefore were necessarily observed in Small Window mode in both the EPIC-MOS and the EPIC-pn cameras. In several cases the core of the Point Spread Function is affected by severe pile-up, and has to be excised. This yields a reduction of the useful count rate for spectral analysis, while also introducing a potential source of systematic uncertainty on the spectral parameters determination due to the larger weight of the comparatively more poorly modeled wings of the PSF in the calculation of the encircled energy fraction correction. On the contrary, most of the 2XMM sources are below the pile-up limit, and were observed using the more frequent Full Frame or Large Window modes. In order to reduce further systematic uncertainties due to pile-up, we have rejected from the 2XMM sub-sample all sources whose count rate exceeded the Full Frame pile-up threshold (cf. the XMM–Newton User's Handbook): 5 counts per second in the EPIC-pn, and 0.7 counts per second in the EPIC-MOS.

The cross-calibration constraints that each 2XMM source carries are on the other hand comparatively smaller. A 2XMM cross-calibration exercise makes sense only if a sufficiently large sample is built. Our 2XMM cross-calibration sub-sample comprised all 2XMM sources fulfilling the following criteria: a) off-axis angle ≤2'; b) number of source counts >1000 in each EPIC camera. The total sample amounts to 285 sources. We extracted source and background spectra, response matrices and effective areas using SASv10.0. We adopted the scientific product spatial extraction regions defined for the compilation of 2XMM (and propagated into an extension of the 2XMM spectral files). Source spectra were re-binned in order to have a minimum of 25 background-subtracted counts in each spectral channel, in order to ensure the applicability of the χ^2 goodness-of-fit test.

The spectra have been analysed using simple photoelectrically absorbed power law models to determine fluxes and spectral shapes. Fits have been separately performed in each of the XCAL energy bands, as well as in the 0.2–2 keV and 2–10 keV energy bands. However, we have retained for the posterior statistical analysis only results derived from "good quality" fits. The threshold to consider a fit good has been arbitrarily set to $\chi^2/\nu < 2$. Moreover, we will consider in the following only measurements of the flux or of the spectral index whose relative error is <25%. The number of measurements fulfilling the above criteria largely varies depending on the energy band, and in the softest XCAL energy band only a few data points satisfy these criteria.

In Fig. 10 the distributions of the MOS/pn flux ratios in the XCAL energy bands are shown. This ratio follows the general trend already observed by analysing the brightest sources in the XCAL database, with values ≃1.07–1.09 in the hardest energy band. The median of the corresponding deviation in spectral index in the 2–10 keV energy band is ≤ 0.05, although the spread of the spectral index differences is rather large, and depending on the exact spectral shape of each individual source (Fig. 11).

The MOS/pn flux ratios do not show any evidence for being time-dependent once the response files
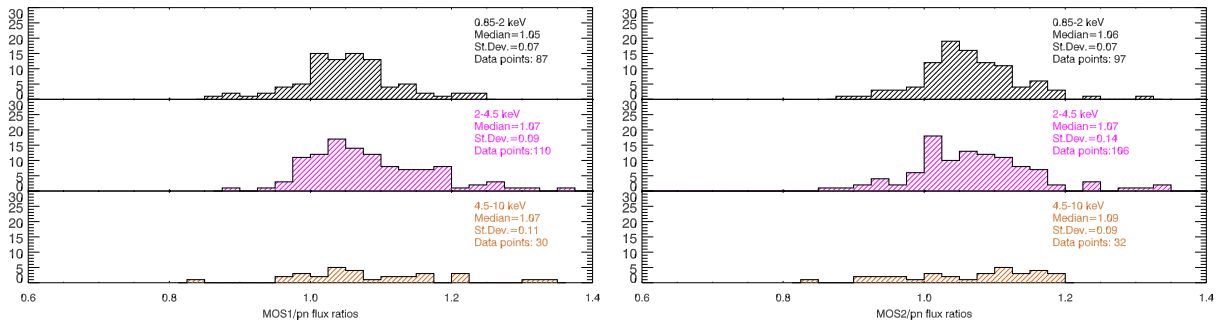

Figure 10: Distribution of MOS1/pn (*left panel*) and MOS2/pn (*right panel*) flux ratios in the XCAL energy bands in the 2XMM on-axis sources sub-sample

european space agency
agence spatiale européenne

Issue/Rev.:   6.0
Date: 23 December 2010

XMM Science Operations Team

Page: 14

appropriate for each source are consistently calculated (Fig. 12).

In summary, the evaluation of the EPIC cross-calibration quality with the 2XMM catalogue sources substantially confirms the XCAL findings. This demonstrates that no mode- or rate-dependent bias is introduced by the source selection in the XCAL.
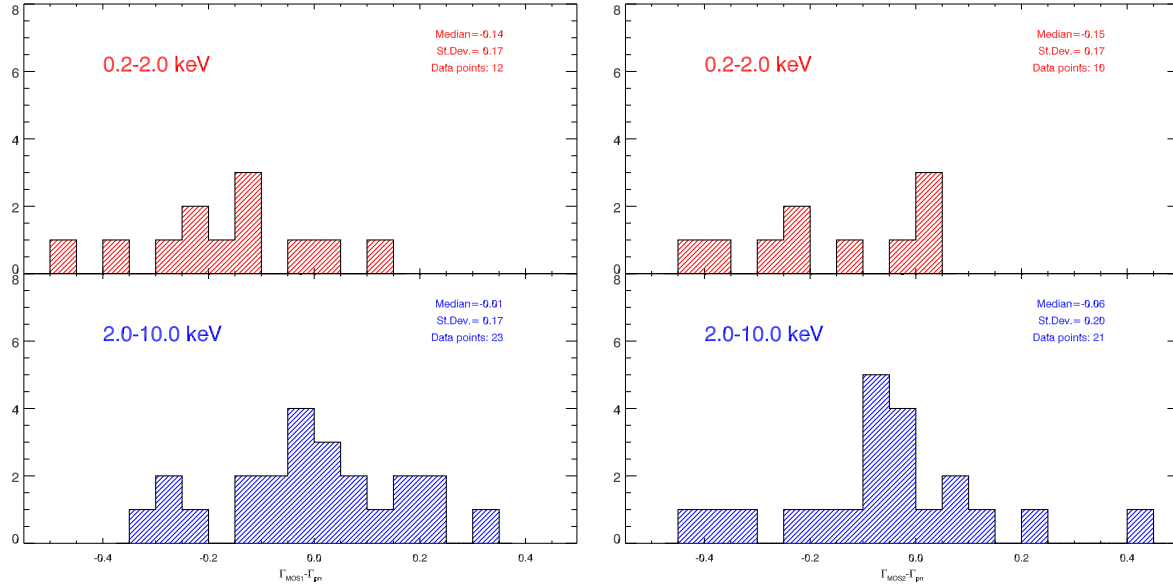
Figure 11: Distribution of the MOS versus pn spectral index differences in the 2XMM on-axis sources sub-sample for the 0.2–2 keV (*upper panels*) and the 2–10 keV (*lower panels*) energy bands. MOS1: *left panel*; MOS2: *right panel*.

Figure 12: MOS/pn flux ratios for the 2XMM on-axis sources sub-sample as a function of observation time (MOS1: *left panel*; MOS2: *right panel*). The *labels* indicate the difference in χ^2 between a fit of the data point with a constant, and with a constant plus a power-law excess at the beginning of the mission. The *dashed* line marks the average of the ratio distribution.

european space agency
agence spatiale européenne

Issue/Rev.: 6.0
Date: 23 December 2010

XMM Science Operations Team

Page: 15

8 Cross calibration of the Optical Monitor filters and grisms

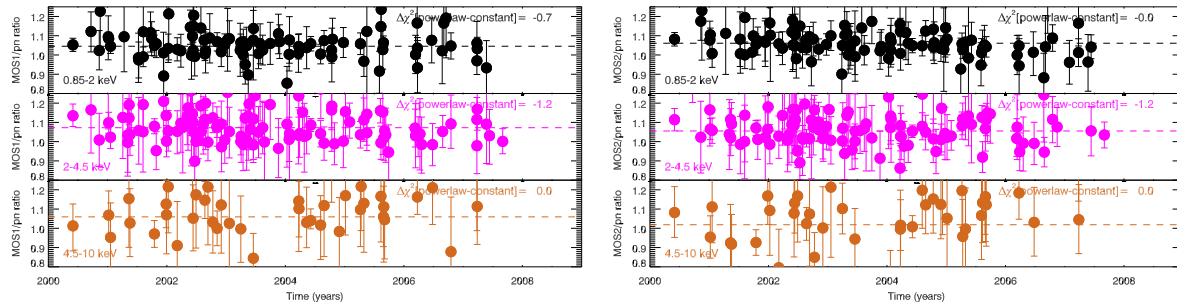The OM instrument has been calibrated with two different approaches: classical photometry performed on images obtained with its broad band filters and absolute flux calibration for filters and grisms.

8.1 OM classical photometry

An instrumental photometric system has been defined and applied to provide aperture photometry of sources detected in images obtained with OM using its different broad band filters. This system allows the user to convert the source measured counts into a magnitude.

For the optical filters (U, B and V), observations of two rich fields with OM and from the ground in the Johnson UBV system have allowed us to define colour transformations to convert the OM instrumental magnitudes into standard UBV.

Several photometric standard fields have been also observed with OM to assess the validity of the transformations. The comparison is very good, with deviations from the standard magnitudes of the order of a hundredth of a magnitude.

The situation is different in the ultraviolet filters (UVW1, UVM2 and UVW2) since there is no photometric standard system for the UV. Recently we have defined for OM an AB magnitude system. This is the closest form to a standard, and therefore some modern instruments working in the UV range are adopting it. Table 2 shows a comparison of the AB magnitudes obtained with OM, GALEX and literature values for a few stars. We should note that the bandpass of OM filters is not exactly the same as those of Galex.

Table 2: OM magnitudes in AB system for a number of reference sources.

star	OM filter	lambda (Å)	AB_OM	AB_Oke 1974	Galex(2271 Å)
HZ 2	U	3440.	13.66	13.74	
	B	4500.	13.66	13.72	
	V	5430.	13.83	14.04	
LBB227	V	5430.	15.27	15.24	
G93-48	UVW2	2120.	12.37		
	UVM2	2310.	12.38		12.39
	UVW1	2910.	12.54		
HZ43	UVW2	2120.	11.24		
	UVM2	2310.			11.36
	UVW1	2910.	12.71		
BD+33 2642	UVW2	2120.	10.43		
	UVM2	2310.	10.45		10.47
	UVW1	2910.	10.38		

8.2 Absolute flux calibration for OM filters and grisms

Real flux in physical units is very convenient in astronomy since it allows direct comparison with models and also with measurements made with different instruments. This is why we have made an attempt in OM to define a direct conversion from measured counts to absolute flux received from the source.

In addition to the filters, the OM instrument is equipped also with two grisms covering respectively the ranges 1800 – 3600 Å (UV grism) and 3000 – 6000 Å (Visible grism). All these elements have been calibrated in flux.

The conversion factors from measured count rate (aperture photometry with the broad band filters) to flux at the effective wavelength of the filters, and the inverse sensitivity function (ISF) of the grisms (a function of wavelength that converts the count rate in the extracted spectrum into absolute flux) have been computed by observing spectrophotometric standard stars, whose flux is well known, with OM.

The count rate to flux conversion factors derived for the broad band filters should apply strictly only for sources with the same spectral shape as the standard stars. For sources with different spectral shape

european space agency
agence spatiale européenne

Issue/Rev.: 6.0
Date: 23 December 2010

XMM Science Operations Team

Page: 16

Table 3: Count rate to flux conversion for OM broad band filters

filter	V	B	U	UVW1	UVM2	UVW2
effective wavelength [Å]	5430	4500	3440	2910	2310	2120
factor ($erg/cm^2/count/\mathring{A}$)	2.49E-16	1.29E-16	1.94E-16	4.76E-16	2.20E-15	5.71E-15
error	0.02	0.07	0.05	0.07	0.04	0.06

correction factors should be obtained (analogous to colour correction) to give accurate results. However, synthetic photometry using different spectral libraries and models and observations performed with OM have shown that the spectral dependence of the conversion factors is in fact very small (except perhaps for sources with strong emission lines) and the factors obtained from the standard stars can be applied to obtain fluxes with errors smaller than 10% in the optical range and smaller than 20% in the UV (for red, emission line sources).

Six standard stars have been used to derive the conversion factors for the broad band filters given in Table 3.
Count rates multiplied by these factors give the fluxes at the effective wavelength of the filter ($erg/cm^2/s/\mathring{A}$). The conversion factors have been obtained from OM data of the standard stars processed with SAS and therefore they include a correction for time sensitivity degradation of the OM detector.

Two standard white dwarfs have been used to derive the ISF of the OM grisms as:

$$ISF = Standard\_flux/OM\_spectrum\_count\_rate$$

therefore

$$CalibratedFlux = Observed\_spectrum\_count\_rate \times ISF$$

Fluxes obtained from OM grisms data with SAS and this calibration agree in general within 10% with values given in the literature. For standard stars we have agreements within 5% in the UV grism and 10% in the Visible grism. In very noisy spectra, or at the shortest wavelength of the UV and the longest one in the Visible, discrepancies can reach 20% level.

The grisms overlap between 3000 – 3600 Å. Calibrated spectra of the same source in this common range agree within 5%.

We have compared the fluxes obtained from aperture photometry in the broad band filters as described above, with OM calibrated grism spectra of the same sources. The agreement is within 10%.

Figure 13 shows the spectrum of the white dwarf standard star BPM 16274 obtained with OM, compared with its corresponding standard flux. The flux observed in each OM filter, after converting count rates to flux, is shown also in this figure.

Figure 14 shows observations of 3C 273 with OM. All filters (except UVM2) and both grisms were used. The agreement quoted above between grisms and filters is again clearly demonstrated.

european space agency
agence spatiale européenne

Issue/Rev.: 6.0
Date: 23 December 2010
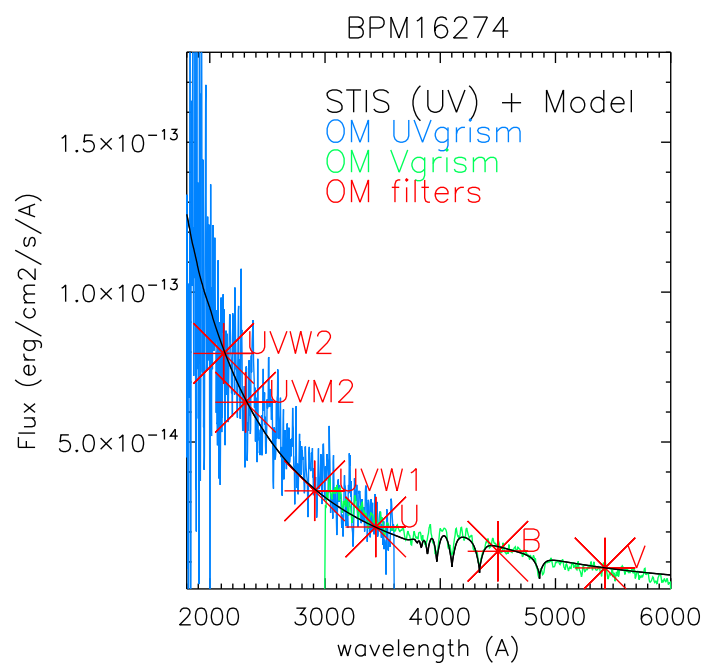
XMM Science Operations Team

Page: 17

Figure 13: Flux calibrated spectrum of the white dwarf BPM 16274, obtained with the OM grisms and all broad band filters

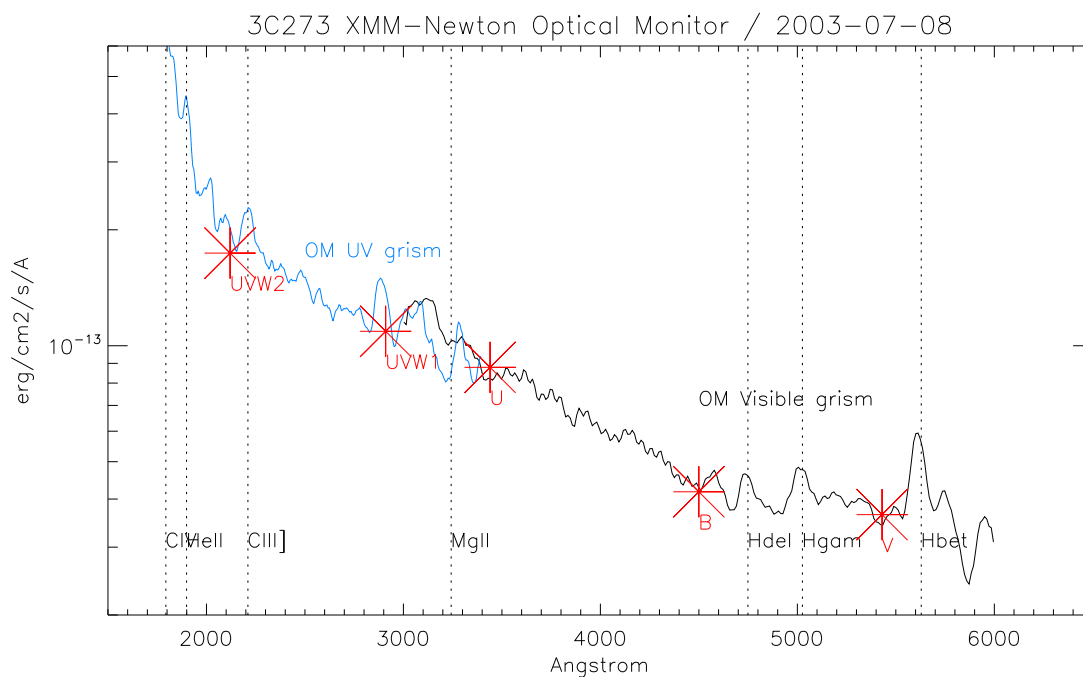Figure 14: OM observations of 3C 273. Red-shifted emission lines are indicated

european space agency
agence spatiale européenne

Issue/Rev.: 6.0
Date: 23 December 2010

XMM Science Operations Team

Page: 18

9 Cross-calibration of XMM–Newton and Chandra

9.1 Blazar sample statistics

The XMM–Newton SOC maintains a XMM–Newton/Chandra cross-calibration archive containing currently 31 simultaneous observations of bright blazars. All Chandra observations are executed with gratings to avoid pile-up effects and the spectra are extracted using merged GTI files, forcing strictly simultaneous exposure times. Chandra data were extracted following standard CIAO threads using version CIAOv4.2 with the CALDB 4.2.2. The fits to the Chandra grating spectra are done on the combined ± first orders. Example spectra of two observations are presented in appendix B.

The fluxes are calculated for a joint fit of all detectors as well as individually for each detector using single power law approximations within limited narrow energy bands. Again, the joint fits in general are driven by EPIC-pn.

These energy bands are 0.15-0.33 keV, 0.33-0.54 keV, 0.54-0.85 keV, 0.85-1.5 keV, 1.5-4.0 keV and 4.0-10.0 keV. For the fits, the recommended individual energy limits of the instruments are taken into account.

Fig. 15 presents the flux ratios of the individual instruments with respect to the joint fits, averaged over all observations. The error bars represent the standard deviation of the mean. For clarity, XMM–Newton instruments are shown in the top panel and Chandra configurations in the lower panel. The dotted vertical lines indicate the different energy bands mentioned above.

Above ∼0.5 keV, ACIS-S LEG & HEG show a flux excess of about 0-10% compared to EPIC-pn and 0-5% compared to EPIC-MOS fluxes. At lowest energies, the ACIS-S LEG mean flux ratios indicate a flux deficit with respect to the joint fit fluxes. Analysis showed that this deficit is mainly due to the negative first order data.

Below 0.3 keV, HRC-S LEG shows a flux deficit of 5-10% compared to EPIC-pn, and above ∼1.5 keV an excess of 10-20%.
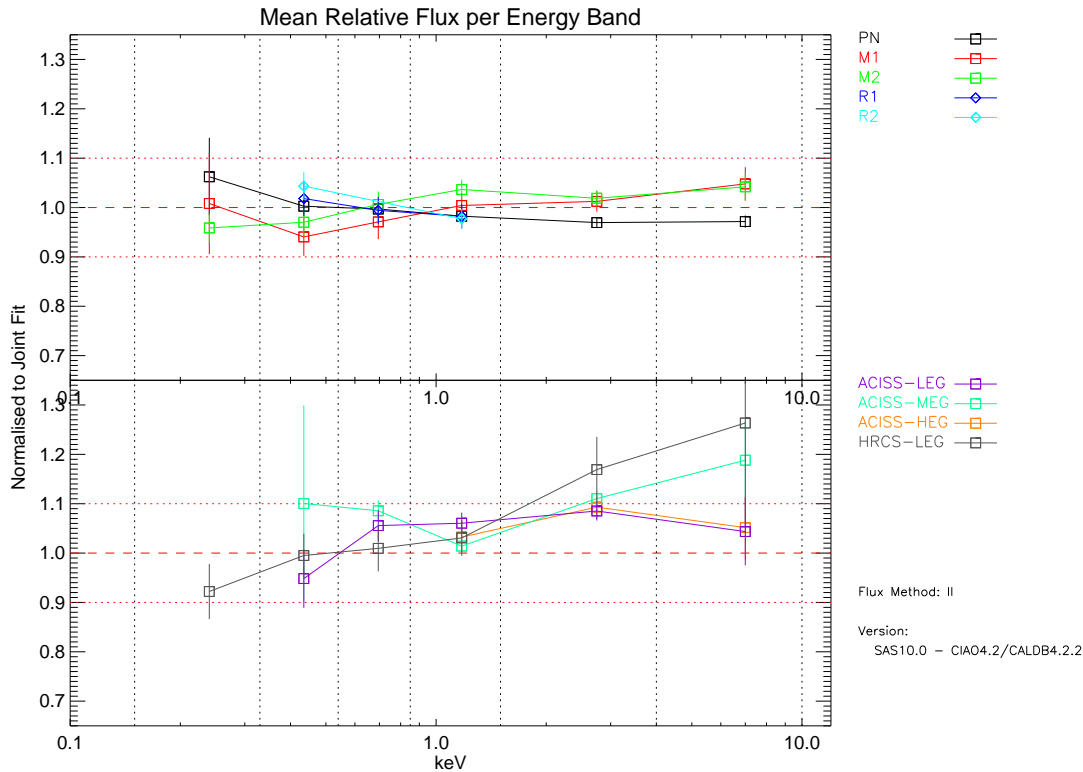

Figure 15: Flux ratios of the individual instruments with respect to the joint fits, averaged over all observations, per energy band. *Top panel*: XMM–Newton instruments, *bottom panel*: Chandra instruments.

european space agency
agence spatiale européenne

Issue/Rev.:   6.0
Date: 23 December 2010

XMM Science Operations Team

Page: 19

10   Summary of IACHEC cross-calibration publications

The International Astronomical Consortium for High Energy Calibration (IACHEC) aims to provide standards for high energy calibration and supervise cross calibration between different missions. This goal is reached through working groups, where IACHEC members cooperate to define calibration standards and procedures. The scope of these groups is primarily a practical one: a set of data and results (eventually published in refereed journals) will be the outcome of a coordinated and standardised analysis of references sources ("high-energy standard candles"). Past, present and future high-energy missions can use these results as a calibration reference.

10.1   J. Nevalainen et al: Cross-calibrating X–ray detectors with clusters of galaxies: An IACHEC study

The IACHEC cluster group has carried out a study of the cross-calibration accuracy of XMM–Newton EPIC, Chandra ACIS and BeppoSAX MECS instruments using clusters of galaxies. The results have been published by J. Nevalainen, L. David, M. Guainazzi, 2010, A&A, (accepted for publication, preprint 2010arXiv1008.2102N). The work is based on CIAO 4.2 with CALDB 4.2.0 and SASv9.0 with CCFs as of December 2009. **Please note that this work could not take into account the latest update of the EPIC-pn redistribution.**

No systematic difference in the temperatures obtained by fitting the 2-7 keV energy band with ACIS and EPIC (2-10 keV for MECS) are found. These values are also consistent with those obtained by the EPIC temperature measurements based on the FeXXV/FeXXVI line ratio. This shows that the energy dependence of the effective area in this band is accurately modelled in all studied instruments.

On the other hand there are systematic calibration uncertainties in the 2-7 keV effective areas at the 6-25 σ level, corresponding to a percentage difference of 5-10%.

The temperatures obtained by fitting the soft band (0.5-2.0 keV) data of EPIC-pn and ACIS differ systematically and significantly, by $\sim$18% (i.e. 8.6 σ level), on average. Due to the higher effective area and higher number of intrinsic cluster photons, the calibration uncertainties of the soft band will affect the scientific analysis of clusters of galaxies when using the full useful energy range ($\sim$0.5-7.0 keV). Considering the variation between the different instruments, the 0.5-7.0 keV band temperature measurements in clusters of galaxies with EPIC/XMM–Newton and ACIS/Chandra is uncertain by 10-15% on average.
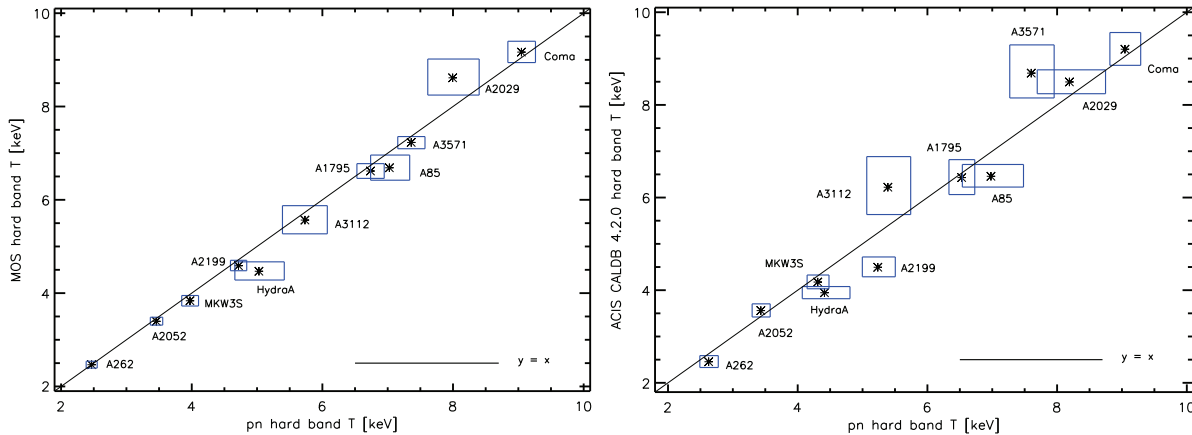

Figure 16: Cluster temperatures obtained by fitting the 2-7 keV energy band. Good agreement of all temperatures.

european space agency
agence spatiale européenne

Issue/Rev.: 6.0
Date: 23 December 2010

XMM Science Operations Team

Page: 20

10.2 M. Tsujimoto et al: Cross-calibration of the X–ray instruments on-board Chandra, INTEGRAL, RXTE, Suzaku, Swift and XMM–Newton observatories using G21.5-0.9

The IACHEC non-thermal SNR group has carried out a study of the cross-calibration accuracy of various instruments on current X–ray observatories using SNR G21.5-0.9. The results have been published by M. Tsujimoto et al, 2010, A&A, (accepted for publication, preprint arXiv:1009.2812v1).

A coherent spectral fitting was conducted with the methods as common as possible for data of Chandra ACIS-S3, INTEGRAL IBIS-ISGRI, RXTE PCA, Suzaku XIS and HXD-PIN, Swift XRT and XMM–Newton EPIC. Many systematic differences are identified, unattributable to statistical uncertainties alone. Most differences are consistent with those reported in previous studies of a similar purpose.

In Fig. 17 we show the comparison among the spectral parameters obtained for the instruments analysed in this paper.
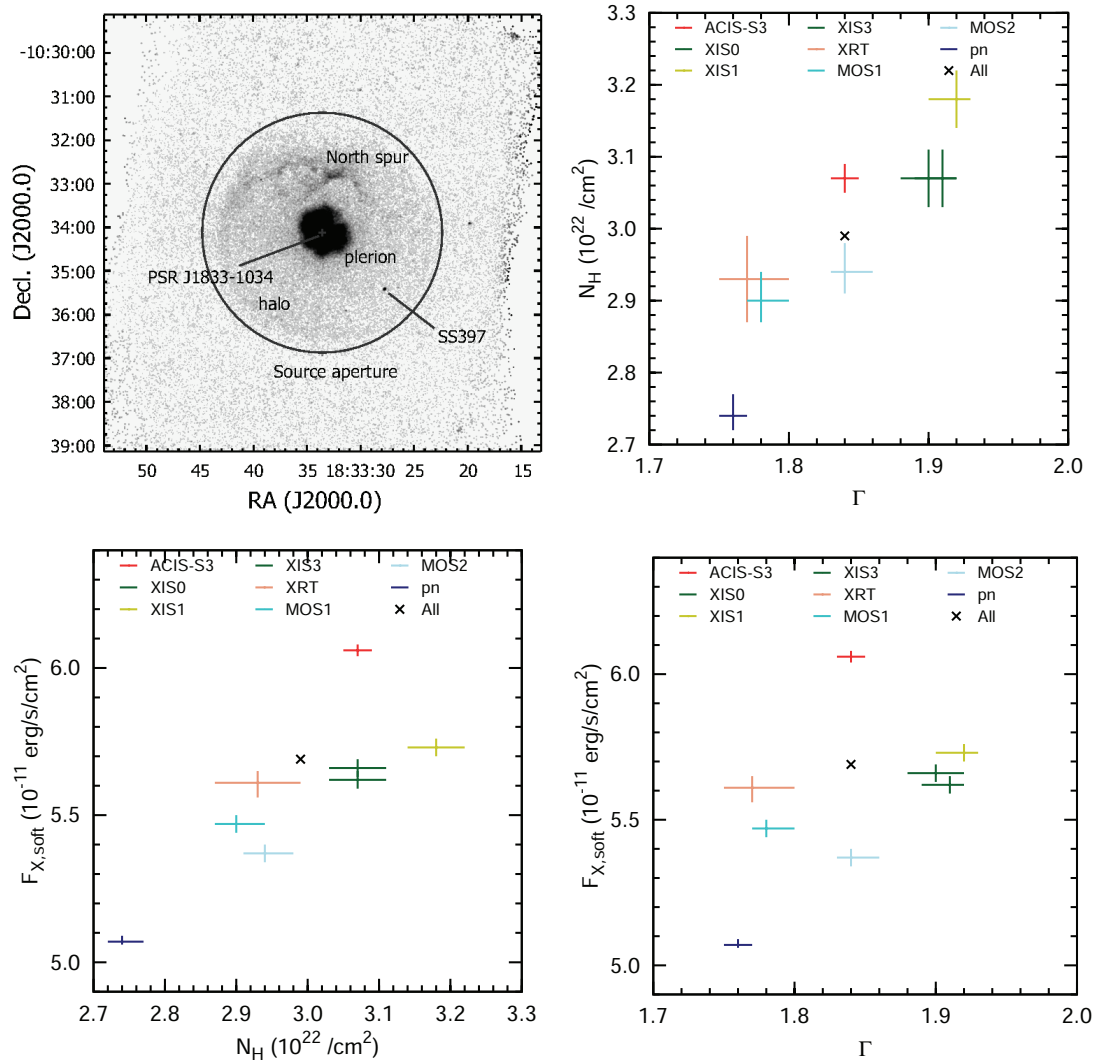

Figure 17: G21.5-0.9 cross-calibration study for various instruments on current X–ray observatories. Many systematic differences identified.

european space agency
agence spatiale europ enne

Issue/Rev.: 6.0
Date: 23 December 2010

XMM Science Operations Team

Page: 21

A   Examples for XMM–Newton EPIC/RGS cross-calibration

The effects of the new RGS contamination model and the EPIC-pn redistribution changes are presented using series of two example sources, the quasar 3C 273 as a continuum source, and 1E0102.2-7219 as a emission line source. In addition to these, more examples in Sect. A.3–A.7 using various sources at different epochs demonstrate the current status of the EPIC/RGS cross–calibration using SASv10.0. All figures show joint fits for all five X–ray instruments, and thus use the identical set of model parameters without normalisation constants. Details can be found with the calibration review tool at the XMM–Newton SOC web page http://xmm2.esac.esa.int/cgi-bin/ept/preview.pl.

A.1   Example continuum source at different epochs: QSO 3C 273

A series of 3C 273 observations for different epochs during the mission is presented in Fig. 18 and Fig. 19, the corresponding best fit parameters of the joint fits are summarised in Tab. 4. All these observations were performed in the EPIC small window modes using the medium filters with exception of rev. 0655 where all EPICs used the thin filters. All examples are joint fits using a double power law and galactic absorption with the absorption column fixed to $N_H = 1.79 \cdot 10^{20}$ cm^{-2}.

The 3C 273 series shows a good general agreement within 10% of all XMM–Newton instruments at all epochs.

The flux ratios and slope differences for individual single power law fits in various narrow energy bands of all 3C 273 observations are presented in Fig. 20 and Fig. 21, respectively. Several 3C 273 observations use EPIC-MOS1 in timing mode for which low energy access is restricted to E>0.3 keV.

At early epochs, the EPIC–MOS normalisations are consistently higher by a few percent than those of the EPIC–pn over the complete energy range. While this remains true for energies above ∼1 keV for all epochs, later epochs at lower energies, where the EPIC–MOS spectra are heavily affected by the redistribution problem due to the patches, show a drop of the EPIC–MOS ratios in comparison with the EPIC-pn.

As can be seen in Fig. 18 and Fig. 19, most observations indicate a step-like feature in the RGS residuals, being typically higher than EPIC-pn below ∼0.5 keV and consistent or slightly below the EPIC-pn ones above ∼0.5 keV. On the other hand, the single power law approximation in narrow bands (Fig. 20) indicate a very good agreement of RGS and EPIC-pn fluxes for the lowest energy band 0.33-0.54 keV, whereas it confirms the few percent lower RGS fluxes for the bands at higher energy.

Table 4: Joint fit parameters of 3C 273 spectra for an absorbed double power law model. Normalisations are given in $[\frac{\text{photons}}{\text{keV cm}^2 \text{ s}}]$ at 1 keV.

	Model: Double power law with galactic absorption			
rev.	Γ1	norm.1	Γ2	norm.2
0096	3.29±0.04	3.0±0.2 · 10^{-3}	1.58±0.01	1.60±0.02 · 10^{-2}
0277	3.04±0.03	7.7±0.3 · 10^{-3}	1.55±0.01	1.83±0.03 · 10^{-2}
0563	3.15±0.08	6.5±0.9 · 10^{-3}	1.71±0.03	2.13±0.09 · 10^{-2}
0655	2.96±0.05	5.5±0.4 · 10^{-3}	1.75±0.01	2.56±0.05 · 10^{-2}
0835	3.34±0.08	2.5±0.3 · 10^{-4}	1.71±0.01	1.65±0.03 · 10^{-2}
1023	3.04±0.05	4.8±0.3 · 10^{-3}	1.54±0.01	1.63±0.03 · 10^{-2}
1299	3.13±0.04	3.5±0.2 · 10^{-3}	1.39±0.01	1.96±0.02 · 10^{-2}
1381	3.14±0.07	2.3±0.3 · 10^{-3}	1.55±0.01	1.73±0.03 · 10^{-2}

european space agency
agence spatiale europ enne

XMM Science Operations Team

Issue/Rev.: 6.0
Date: 23 December 2010

Page: 22

Figure 18: Joint fits of he continuum source 3C 273 at different epochs in revs. 0096, 0277, 0563 and 0655 (top left to bottom right). The observations were performed in EPIC small window mode using the medium filters with the exception of rev. 0655 where all EPICs used the thin filters.

european space agency
agence spatiale europ enne

Issue/Rev.: 6.0
Date: 23 December 2010

XMM Science Operations Team

Page: 23
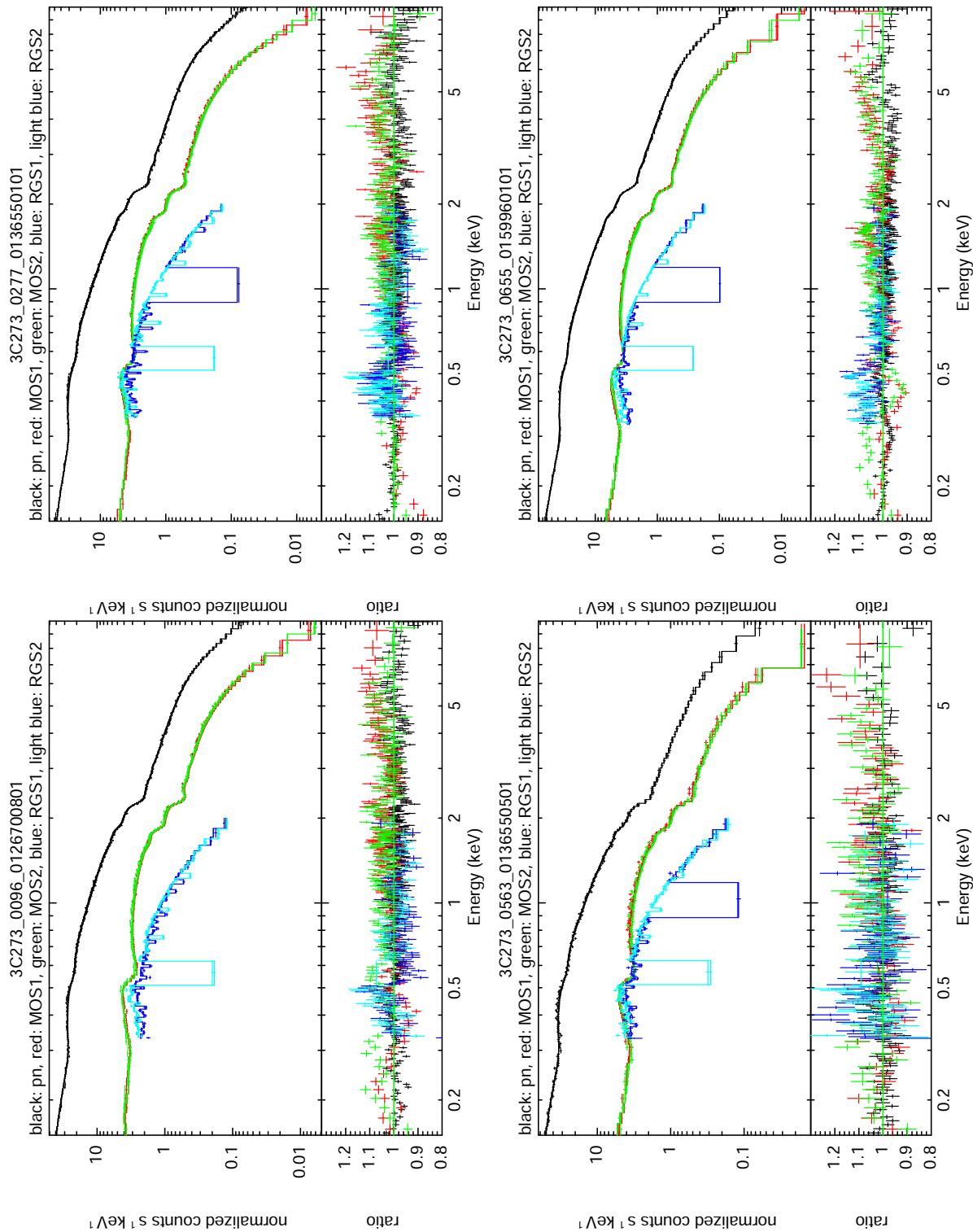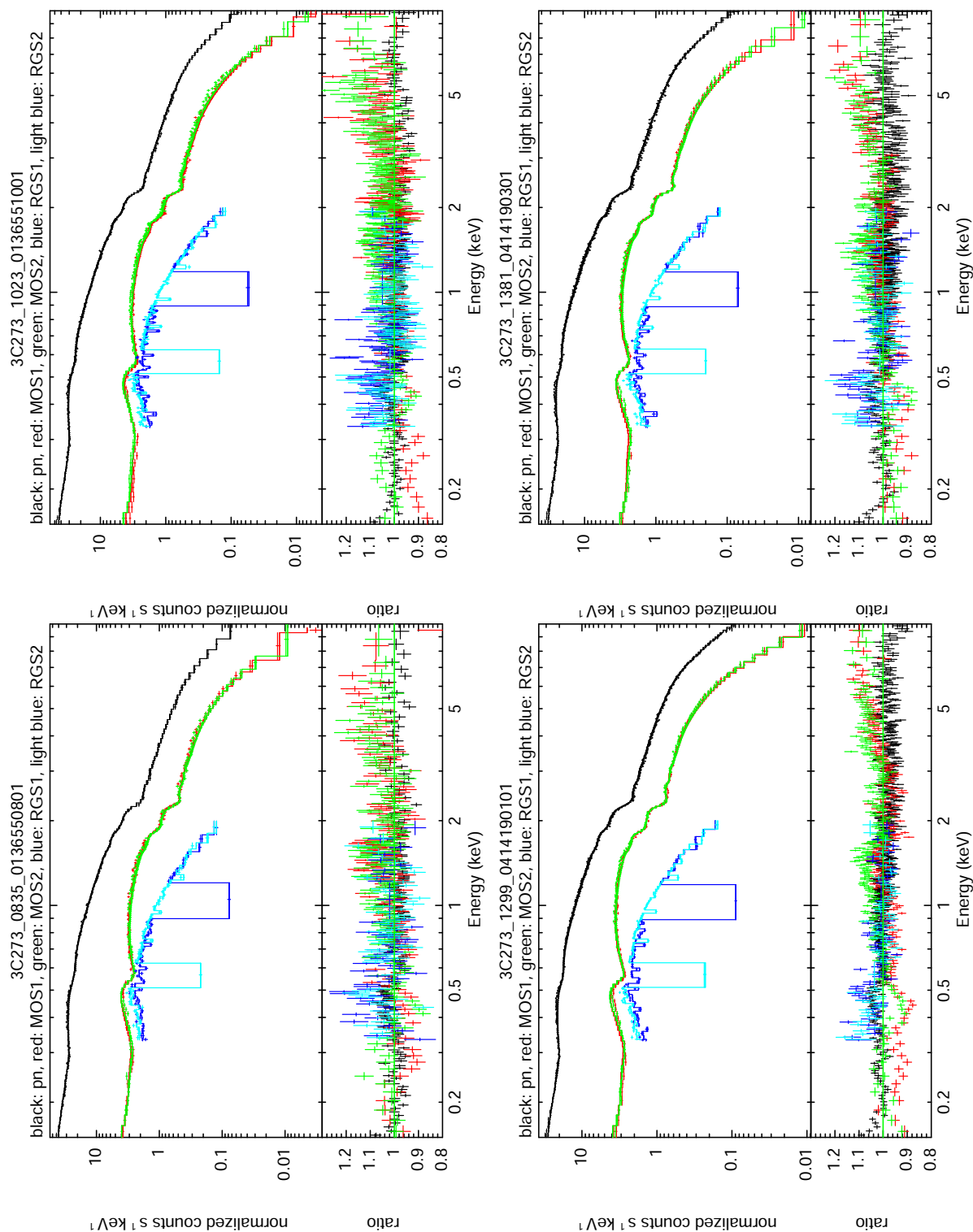
Figure 19: Joint fits of continuum source 3C 273 at different epochs in revs. 0835, 1023, 1299 and 1381, (top left to bottom right). All observations were performed in EPIC small window mode using the medium filters.

european space agency
agence spatiale europ enne

Issue/Rev.: 6.0
Date: 23 December 2010

XMM Science Operations Team

Page: 24

Relative flux ratio history
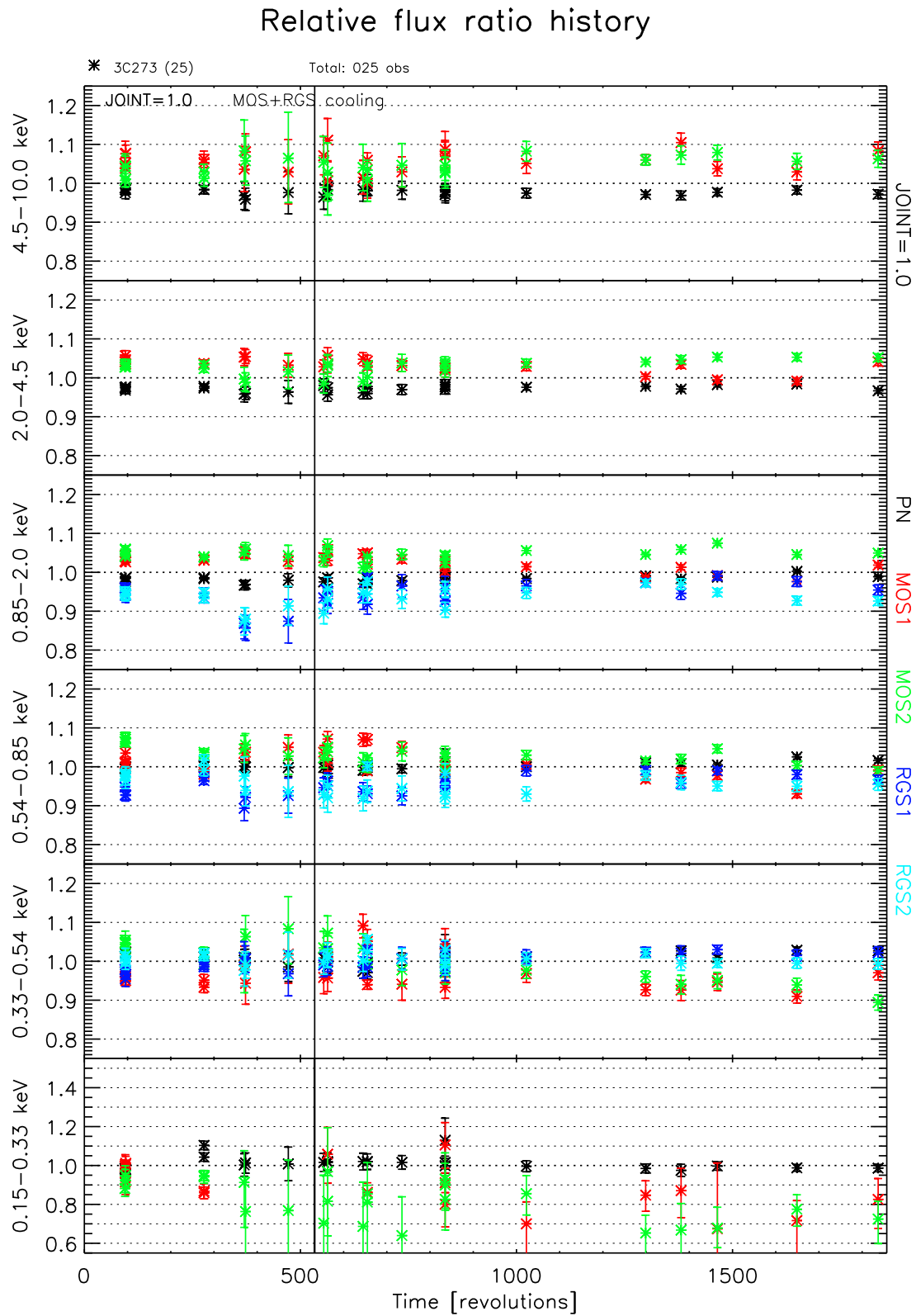
Figure 20: The flux ratios of individual single power law fits in various energy bands for all 3C 273 observations. The fluxes are normalised to the joint fit fluxes.

european space agency
agence spatiale europ enne

Issue/Rev.: 6.0
Date: 23 December 2010

XMM Science Operations Team

Page: 25

Relative slope difference history
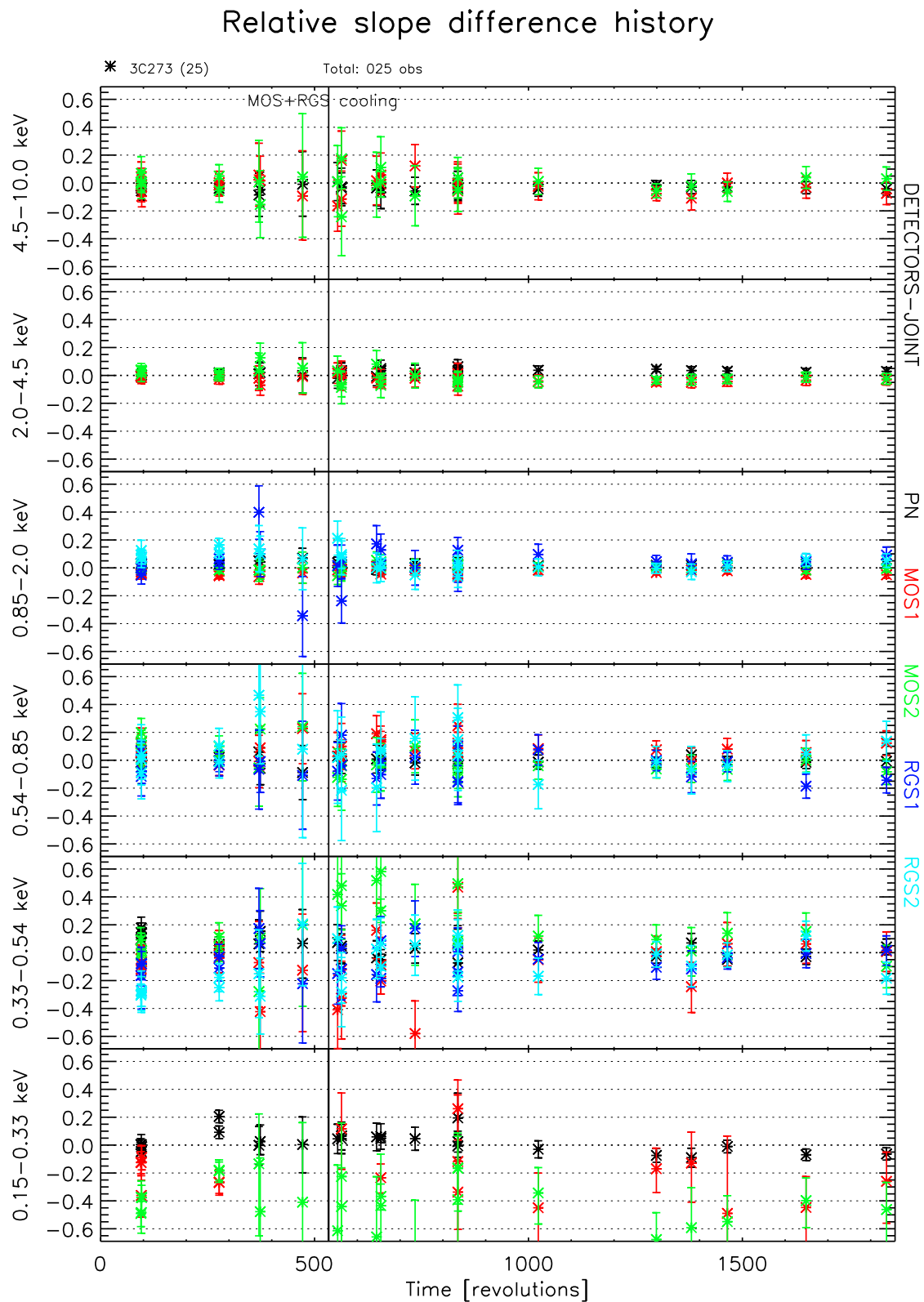

Figure 21: The slope differences of individual single power law fits in various energy bands for all 3C 273 observations. The joint fit slopes are used as reference.

european space agency
agence spatiale europ enne

Issue/Rev.: 6.0
Date: 23 December 2010

XMM Science Operations Team

Page: 26

A.2 Example emission-line source at different epochs: SNR 1E0102.2-7219

For 1E0102.2-7219 the model proposed by the XMM–Newton and Chandra calibration teams within the IACHEC[3] is used. The model includes 52 Gaussian lines with two-temperature continuum, galactic absorption as well as absorption within the Small Magellanic Cloud. For the fit, only 4 free parameters are allowed which are the normalisations for the dominant line complexes of O VII, O VIII, Ne IX and Ne X. All other parameters are fixed according to the best fit constraints of all combined RGS data.

All observations presented in Fig. 22 and Fig. 23 were performed in large window mode for EPIC-MOS. The EPIC-pn observed in small window mode using thin filter with exception of rev 0981 which used large window mode with thin filter. For pn small window mode, the background correction is difficult due to the small size of the CCD window.

The general EPIC/RGS line agreement is good over the complete energy range. The highest residuals typically appear at energies below the O VII complex, where the EPIC spectra are affected by high redistribution. For epochs when the redistribution patch had already undergone a significant evolution, EPIC–MOS show a strong excess between 0.3-0.4 keV. The 1E0102.2-7219 series show signature of a small random gain shift (up to ± 10 eV) in the EPICs.
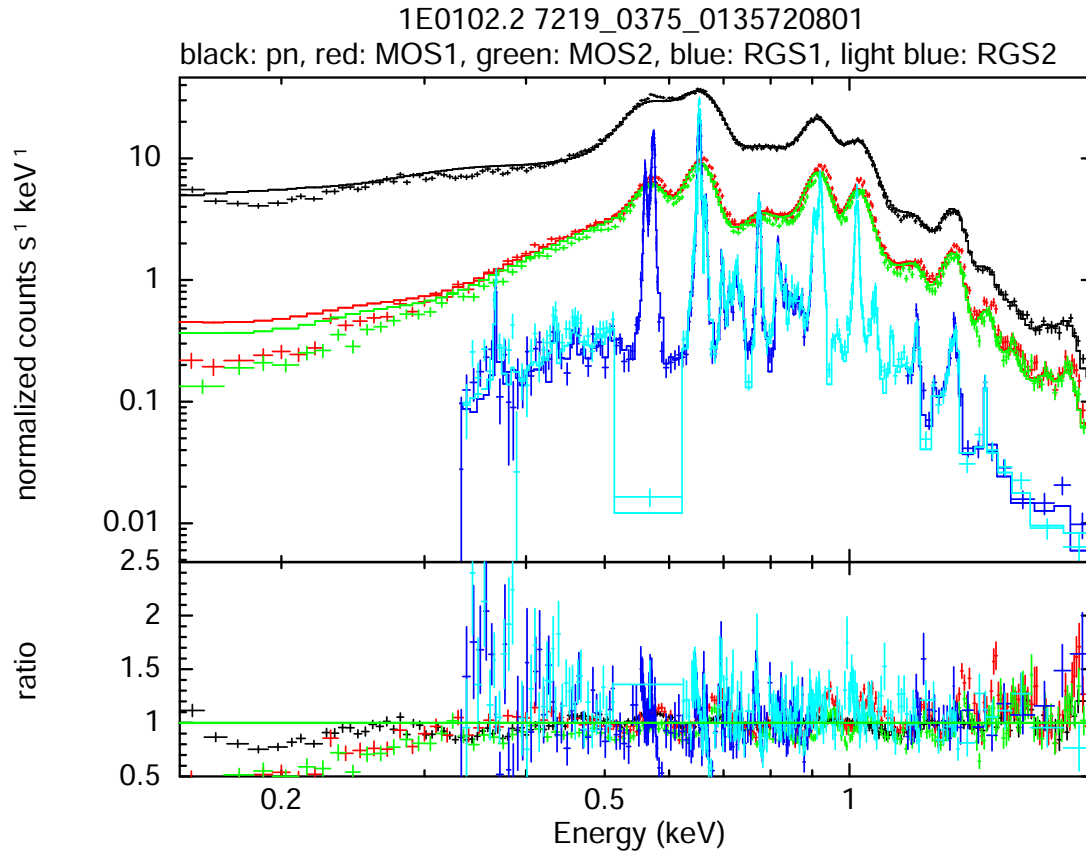

Figure 22: Joint fits of SNR 1E0102.2-7219 in rev. 0375. The observations was performed in large window mode using the thin filter for EPIC-MOS and EPIC-pn observed in small window mode and thin filter.

---

[3]International Astronomical Consortium for High Energy Calibration, http://www.iachec.org

european space agency
agence spatiale europ enne

Issue/Rev.: 6.0

Date: 23 December 2010

XMM Science Operations Team

Page: 27

Figure 23: Joint fits of SNR 1E0102.2-7219 at different epochs in rev. 0981 and 1351(top to bottom). Both observations were performed in large window mode using the thin filter for EPIC-MOS. In rev. 0981 EPIC-pn observed in large window mode and thin filter, in rev. 1351 in small window mode and thin filter

european space agency
agence spatiale europ enne

Issue/Rev.: 6.0
Date: 23 December 2010

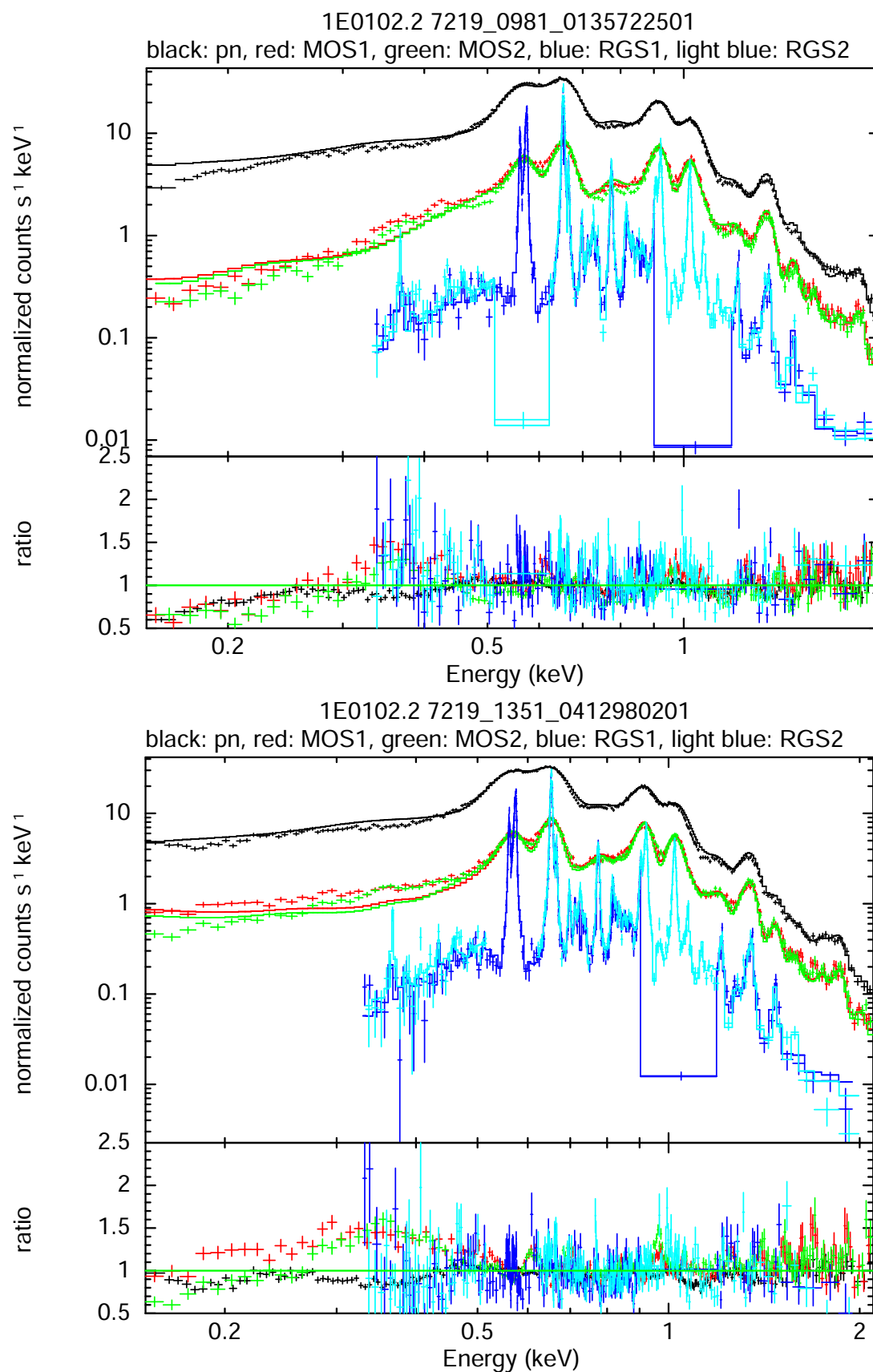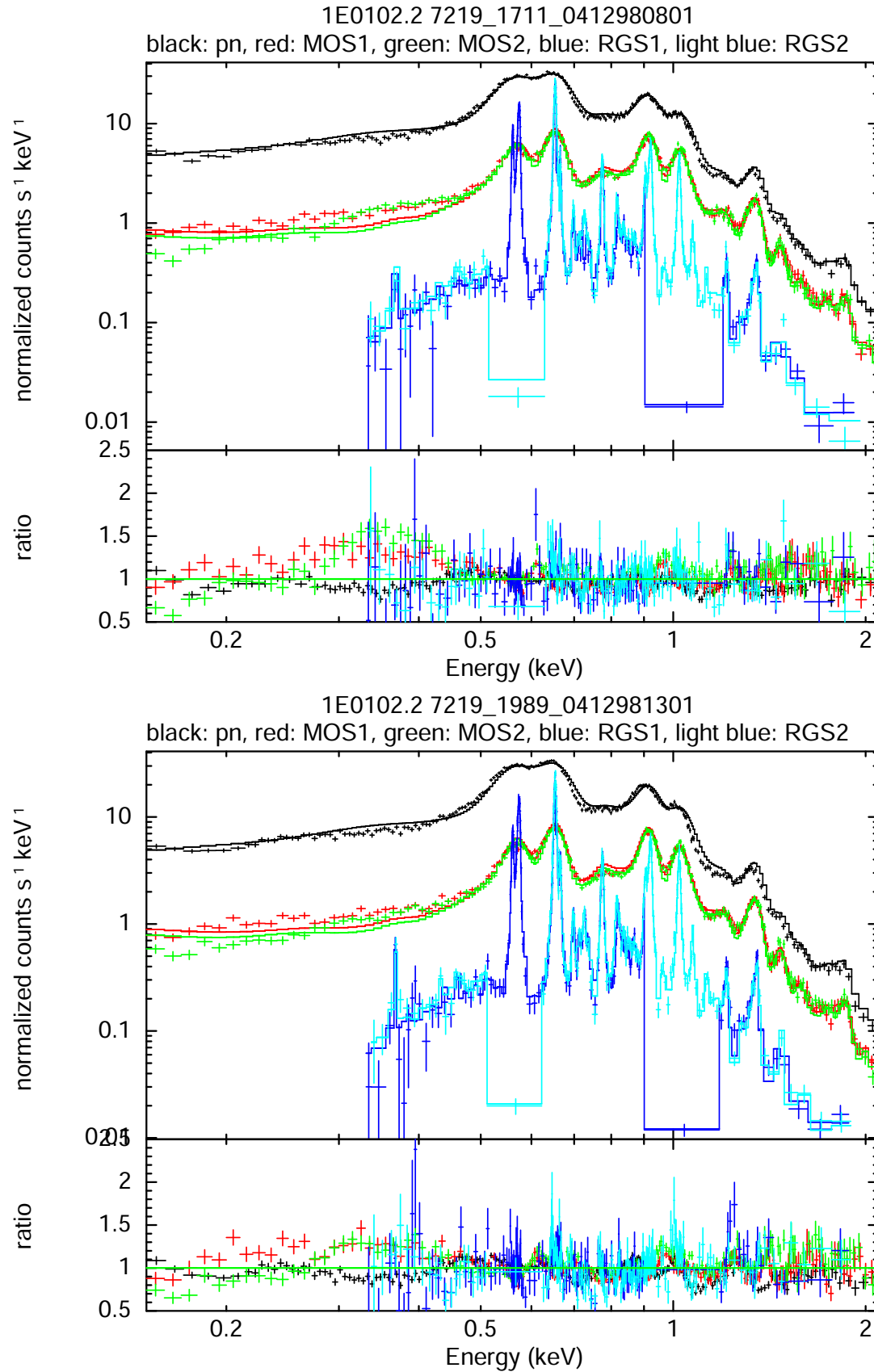**XMM Science Operations Team**

Page: 28

Figure 24: Joint fits of SNR 1E0102.2-7219 at different epochs in rev. 1711 and 1989 (top to bottom). Both observations were performed in large window mode and thin filter for all EPIC-MOS and small window mode and thin filter for EPIC-pn.

european space agency
agence spatiale europ enne

Issue/Rev.: 6.0
Date: 23 December 2010

XMM Science Operations Team

Page: 29

A.3 An early example of MOS pre-patch cross-calibration: Narrow line Seyfert 1 galaxy PKS0558-504

PKS0558-504 (Fig. 25) was observed in rev. 0153, before the MOS patch was present. The pn was in small window mode, MOS in large window mode. All EPICs used the thin filters. This observation is an example of good general agreement between all EPIC and RGS instruments. All spectral parameters agree within 2 σ for all instruments. EPIC-MOS2 fluxes are about 4-5% above those of EPIC-pn. EPIC-MOS1 fluxes agree with EPIC-pn fluxes except in the 0.4-0.7 keV range. RGS fluxes tend to be slightly lower than those of EPIC-pn. All fluxes are consistent within errors.

Table 5: Parameters of the PKS0558-504 joint fit for an absorbed disk black body plus power law model. Normalisations are given in $[(\frac{\text{R/km}}{\text{D/10kpc}})^2 \cos\Theta]$ for the disk black body and $[\frac{\text{photons}}{\text{keV cm}^2 \text{ s}}]$ at 1 keV for the power law.

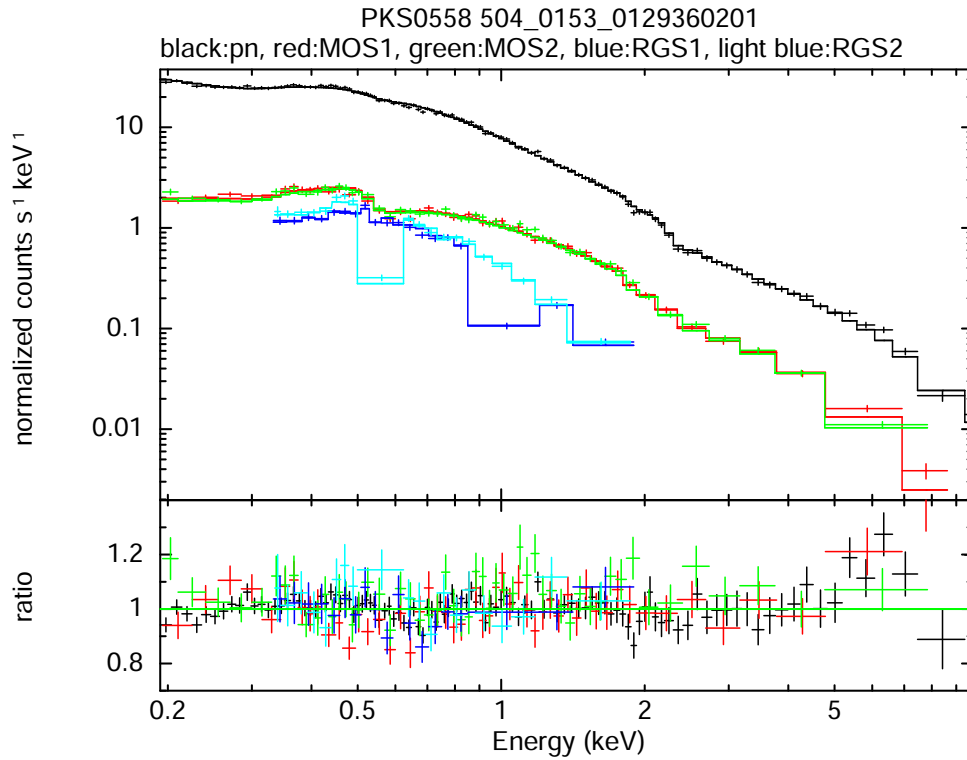|	Model: Disk black body and power law with galactic absorption.				
rev.	N_H [cm^{-2}]	T_{in} [keV]	diskbb norm.	Γ	pl.norm.
0153	$2.4\pm0.2 \cdot 10^{20}$	0.167 ± 0.006	$9.7\pm1.8 \cdot 10^2$	2.20 ± 0.03	$6.0\pm0.2 \cdot 10^{-3}$

Figure 25: PKS0558-504 in rev. 153, before the MOS patch was present. Good agreement is found between all XMM–Newton instruments.

european space agency
agence spatiale europ enne

Issue/Rev.:   6.0
Date: 23 December 2010

XMM Science Operations Team

Page: 30

A.4   BL Lac-type QSO PKS2155-304

At the PKS2155-304 observation in rev. 0545 (Fig. 26) the MOS redistribution patch had already under-gone a significant evolution (with respect to the case shown in the previous section **??**). The observation used the EPIC small window modes with the medium filter.

The ratios show good general agreement over the total energy range. Above $\sim$0.8 keV, EPIC–MOS fluxes are consistently higher than EPIC–pn ones by about 4%. In the $\sim$0.4-0.8 keV range the EPIC-MOS show larger residuals due to the patches. The RGS fluxes are consistent with EPIC-pn below $\sim$0.5 keV and about 3% lower at higher energies.

Both EPIC-MOS agree in their slopes and break energy within 1 σ, normalisations within 3 σ. While the slopes agree within 2.7 σ for EPIC-pn and EPIC-MOS, the instruments disagree significantly for the break energy, which is found E_{break}=0.94$\pm$0.05 keV for EPIC-pn and E_{break}=1.59$\pm$0.08 keV for EPIC-MOS1 (E_{break}=1.45$\pm$0.09 keV for EPIC-MOS2).

For RGS, due to the more limited available energy range, there is no statistical preference of a broken power law over a single power law, both with galactic absorption. The broken power law parameters therefore, especially the break energy, are not well constrained. Nevertheless the low energy slope $\Gamma1$ agrees within 2 σ, with the EPIC results.

Table 6: Parameters of the PKS2155-304 joint fit for an absorbed broken power law model.

	Model: Broken power law with galactic absorption				
rev.	N_H [cm^{-2}]	$\Gamma1$	E_{break} [keV]	$\Gamma2$	norm. [$\frac{photons}{keV\ cm^2\ s}$ at 1 keV]
0545	$1.24 \cdot 10^{20}$ (fixed)	2.604$\pm$0.004	1.40$\pm$0.04	2.864$\pm$0.010	1.925$\pm$0.005 $\cdot 10^{-2}$
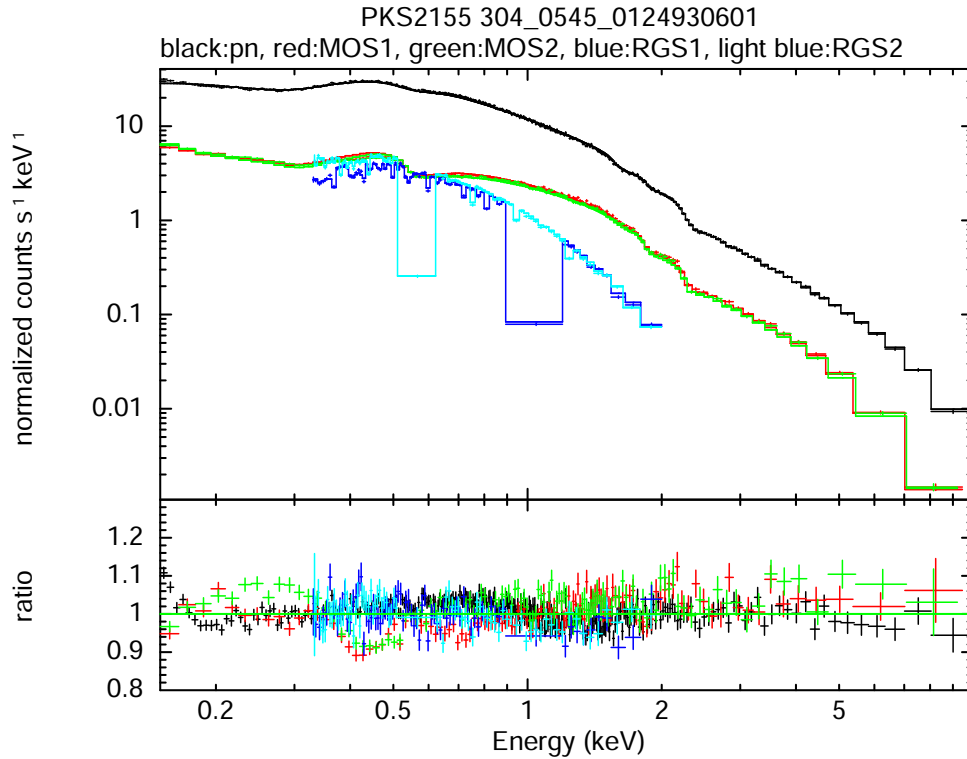
Figure 26: PKS2155-304 in rev. 0545 with MOS patch present. range.

european space agency
agence spatiale europ enne

Issue/Rev.:   6.0
Date: 23 December 2010

XMM Science Operations Team

Page: 31

A.5   Isolated neutron star RXJ1856.6-3754

The isolated neutron star RXJ1856.6-3754 has been observed 13 times within the mission using EPIC small window modes and the thin filters. The neutron star is assumed to have constant X–ray characteristics (within XMM–Newton lifetime) and is therefore used for detector stability analysis.

As presented in Sect. 5, the EPIC-pn fluxes in the 0.15-0.85 keV range are stable within 1%, showing the low-energy stability of the EPIC-pn. Fig. 27 presents the rev. 0878 observation with all EPICs in small window mode using the thin filters. The low-energy spectra for EPIC–MOS strongly depend on the position on the CCDs. Thus the MOS residuals of RXJ1856.6-3754 joint fits can differ significantly between individual observations.

Here, MOS1 suffers from an insufficient patch correction, it deviates up to 15% at lowest energy. In addition both MOS show a dip in their residuals between 0.4–0.5 keV.

EPIC-pn and RGS fit parameters agree within errors, and the two EPIC-MOS temperatures and normalisations agree within errors. EPIC-MOS1 returns a four times higher N_H than EPIC-MOS2. EPIC-pn and EPIC-MOS temperatures agree within 2.5 σ, normalisations within 3 σ. Due to the low N_H, thus rather large error bars, N_H agrees within 2.1 σ.

Table 7: Parameters of the RXJ1856.6-3754 joint fit for an absorbed black body model in the energy range 0.15-0.85 keV.

| rev. | Model: Black body with galactic absorption | | |
	N_H [cm^{-2}]	Temp. [eV]	norm. [$\frac{L_{39}}{D_{10}}$]
0878	$3.0\pm0.4 \cdot 10^{19}$	63.6 ± 0.3	$2.84\pm0.05 \cdot 10^{-4}$
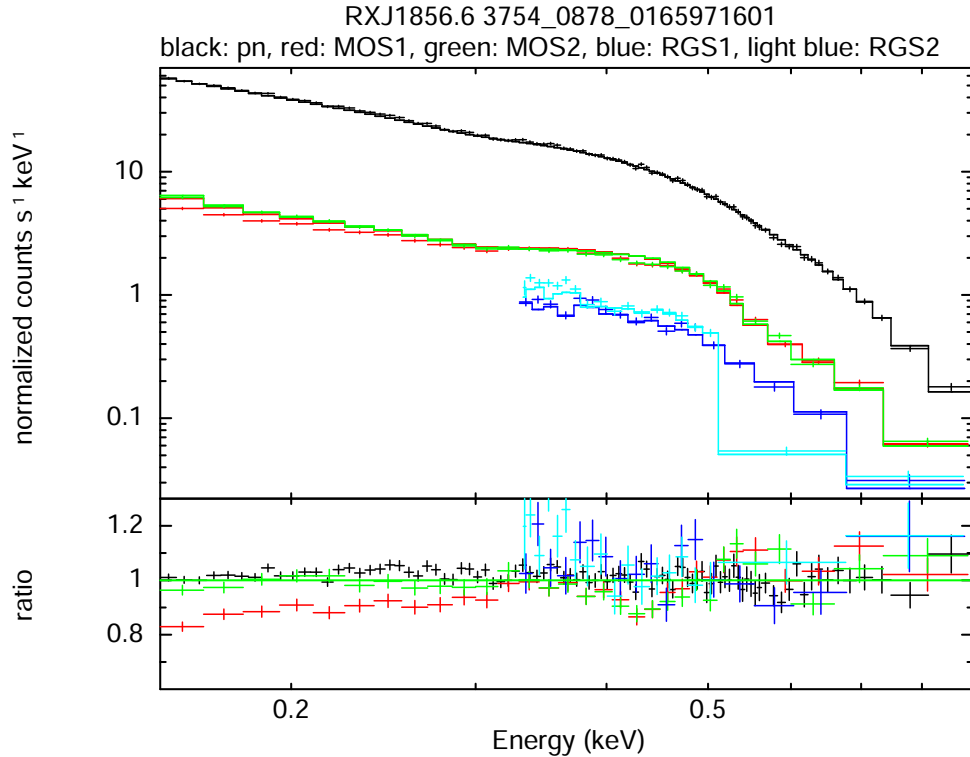
Figure 27: RXJ1856-3754 in rev. 0878. RGS and EPIC-pn parameters were in good agreement.

european space agency
agence spatiale europ enne

Issue/Rev.: 6.0
Date: 23 December 2010

XMM Science Operations Team

Page: 32

A.6 BL Lac-type QSO H1426+428

In rev. 1035, H1426+428 was observed in small window mode with medium filters for all EPICs (Fig. 28).

The spectral slopes are in good agreement for all instruments. The high energy slope and break energies agree within errors for all EPICs. Although the difference in the low energy slope is less than $\delta\Gamma = 0.1$, due to the very small statistical error bars the EPIC-pn ($\Gamma = 2.055 \pm 0.007$) and EPIC-MOS (MOS1: $\Gamma = 1.99 \pm 0.01$; MOS2: $\Gamma = 1.96 \pm 0.01$) are formally inconsistent.

For RGS, there is no statistical preference of a broken power law over a single power law, both with galactic absorption. The broken power law parameters therefore, especially the break energy, are not well constrained. Nevertheless the low energy slope $\Gamma1$ agrees within errors with the EPIC-pn result.

EPIC-MOS fluxes above $\sim$0.8 keV are about 4-5% higher than EPIC-pn fluxes and consistent below. RGS fluxes are consistent with EPIC-pn ones within 3%.

Table 8: Parameters of the H1426+428 joint fit for an absorbed broken power law model.

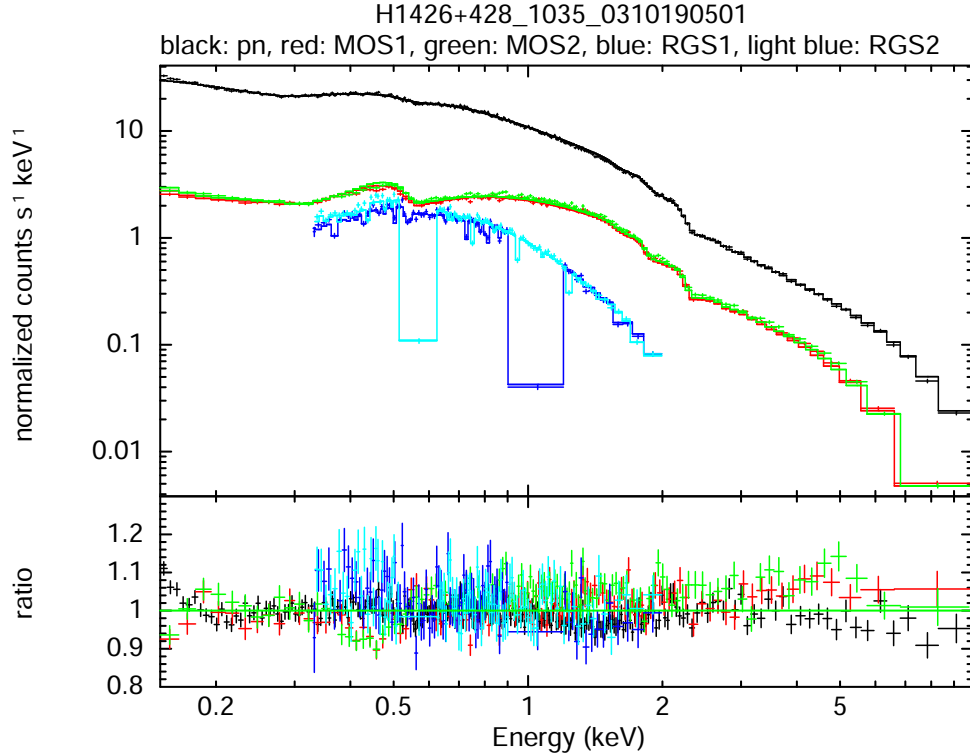|	Model: Broken power law with galactic absorption				
rev.	N_H [cm^{-2}]	$\Gamma1$	E_{break} [keV]	$\Gamma2$	norm. $\left[\frac{photons}{keV\ cm^2\ s}\ at\ 1\ keV\right]$
1012	$1.36 \cdot 10^{20}$ (fixed)	2.035 ± 0.005	1.40 ± 0.05	2.295 ± 0.009	$1.511\pm0.005 \cdot 10^{-2}$

Figure 28: H1426+428 in rev. 1035. All XMM–Newton instruments agree within 10% over the complete energy range.

european space agency
agence spatiale europ enne

Issue/Rev.: 6.0
Date: 23 December 2010

XMM Science Operations Team

Page: 33

A.7 Galaxy cluster A2029

A2029 was observed in rev. 1592 using thin filters and full frame mode for EPIC-MOS and extended full frame mode for EPIC-pn. The redshift of the cluster was fixed to redshift z=0.0773 and the abundance to 0.58 solar. The analysis was done for an annular region of 1.5-2.5 arcmin, for which the cluster spectrum can be described using a single temperature plasma model. As an identical region selection is not possible for the RGS, only EPIC instruments are taken into account.

All fit parameters of EPIC-pn and EPIC-MOS2 agree within 2 σ, with slightly higher temperature and N_H as well as lower normalisation for MOS2. EPIC-MOS1 measures a higher temperature (2.8 σ) and lower normalisation (4 σ) and N_H (2 σ) compared to EPIC-pn.

The EPIC-MOS return slightly lower fluxes below $\sim$2 keV and slightly higher fluxes at high energies.

Table 9: Parameters of the A2029 joint fit for an absorbed single temperature plasma model.

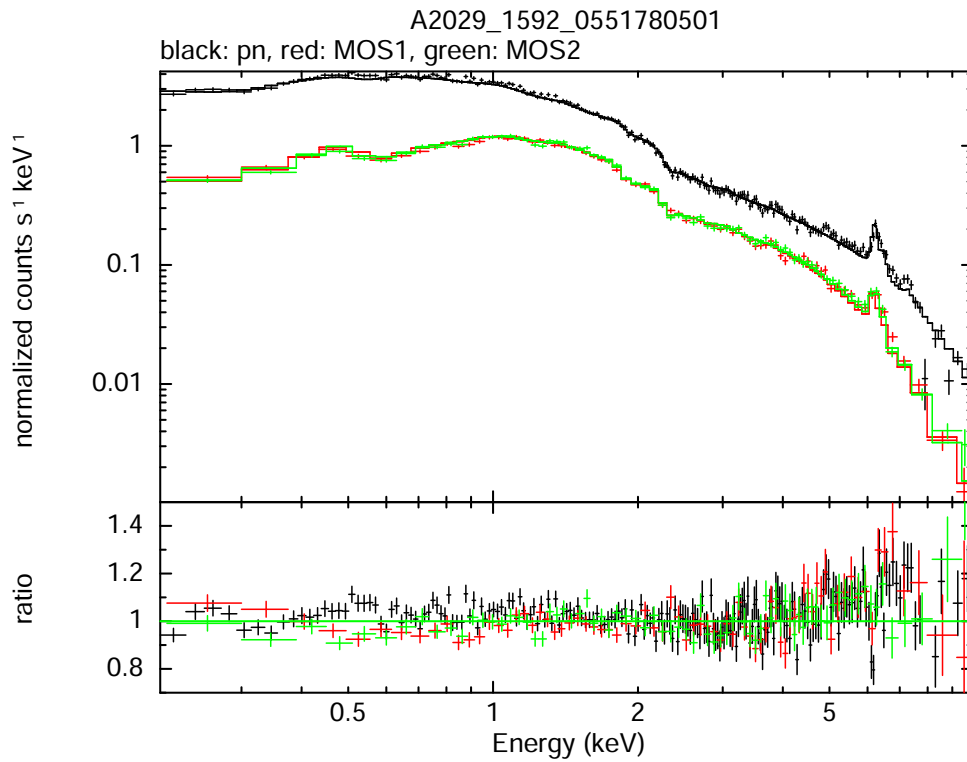| rev. | Model: Diffuse plasma emission (mekal) with galactic absorption. | | | |
	N_H [cm^{-2}]	abund.	T [keV]	norm
1592	$3.5\pm0.1 \cdot 10^{20}$	0.58 (fixed)	7.2 ± 0.1	$1.56\pm0.01 \cdot 10^{-2}$

Figure 29: A2029 in rev. 1592. All individual fit parameters of EPIC-pn and EPIC-MOS2 agree within 2 σ with the best joint fit given in Tab.9.

european space agency
agence spatiale europ enne

Issue/Rev.:   6.0
Date: 23 December 2010

XMM Science Operations Team

Page: 34

B   Examples for XMM–Newton/Chandra cross-calibration

All Chandra observations presented in this section are reduced using CIAO 4.2 and CALDB 4.4.2. The XMM observations are processed using SASv10.0 and the latest CCFs. The model and residuals are determined by joint fits to all instruments. The joint fits in general are driven by EPIC-pn.

B.1   Examples for cross-calibration with Chandra ACIS-S/LEG

The first example presents a simultaneous observation of PKS2155-304 in May 2009 (Fig. 30). In general the spectra measured by XMM–Newton EPIC, RGS and Chandra ACIS-S/LEG agree within 10%. The largest residuals with respect to the joint fit are seen above ∼2 keV for ACIS-S/LEG, and below ∼0.4 keV for the ACIS-S/LEG negative first order. Chandra normalisations are higher than those of EPIC and agree better with EPIC–MOS than EPIC–pn.

Table 10: Parameters of the PKS2155-304 joint fit of XMM–Newton instruments and Chandra using ACIS-S/LEG for an absorbed broken power law model.

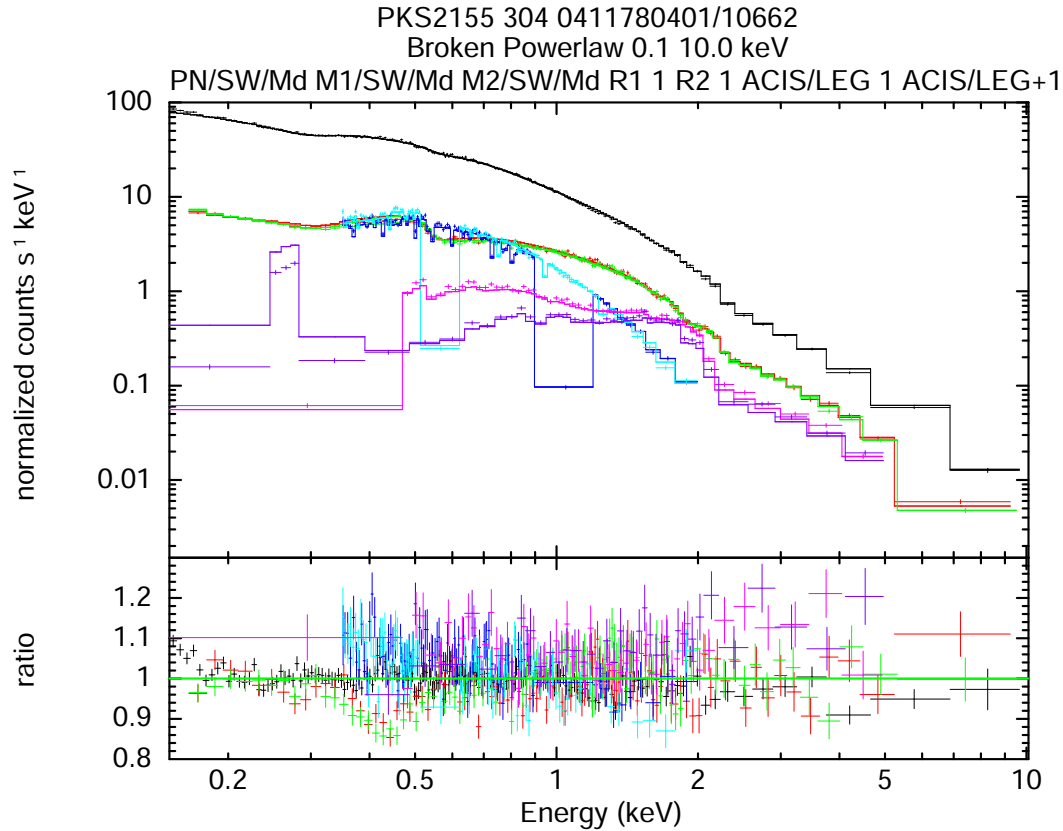| Model: Broken power law with galactic absorption				
N_H [cm^{-2}]	Γ1	E_{break} [keV]	Γ2	norm. [$\frac{photons}{keV\ cm^2\ s}$ at 1 keV]
$1.24 \cdot 10^{20}$ (fixed)	2.695±0.006	1.06±0.07	2.858±0.013	3.20±0.02 · 10^{-2}

Figure 30: Simultaneous XMM–Newton and Chandra observations of PKS2155-304 in May 2009 with Chandra using ACIS-S/LEG. The XMM–Newton spectra are coloured as in the previous figures, Chandra ACIS-S/LEG-1 in purple and ACIS-S/LETG+1 in magenta.

european space agency
agence spatiale europ enne

Issue/Rev.: 6.0
Date: 23 December 2010

XMM Science Operations Team

Page: 35

B.2 Examples for cross-calibration with Chandra ACIS-S/HETG

An example of a simultaneous observation by XMM–Newton and Chandra ACIS-S/HEG and ACIS-S/MEG is presented in Fig. 31. H1426+428 was observed in June 2005. For both Chandra gratings, plus/minus first order are combined within XSPEC.

Between 0.5-2.0 keV XMM–Newton and Chandra instruments agree within 10%. Above 2 keV, the ACIS-S/MEG/HEG residuals are of the order of 20% above the joint fit. Of the EPIC data, those of EPIC-MOS lie closest to ACIS-S/MEG/HEG.

Table 11: Parameters of the H1426+428 joint fit of XMM–Newton instruments and Chandra ACIS-S/MEG/HEG using an absorbed broken power law model.

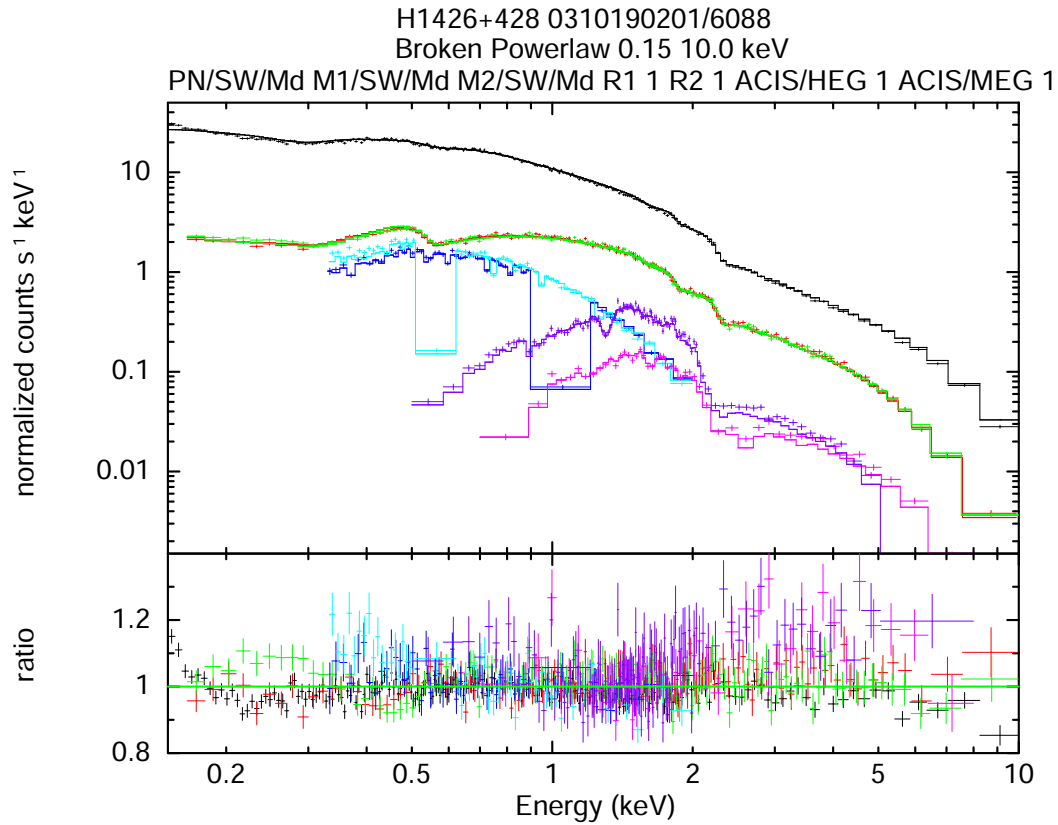| Model: Broken power law with galactic absorption				
N_H [cm^{-2}]	$\Gamma 1$	E_{break} [keV]	$\Gamma 2$	norm. [$\frac{photons}{keV\ cm^2\ s}$ at 1 keV]
$1.36 \cdot 10^{20}$ (fixed)	1.925 ± 0.005	1.41 ± 0.06	2.145 ± 0.009	$1.533 \pm 0.005 \cdot 10^{-2}$

Figure 31: Simultaneous XMM–Newton and Chandra observations of H1426+428 in June 2005 with Chandra using ACIS-S/MEG and ACIS-S/HEG. The XMM–Newton spectra are coloured as in the previous figures, Chandra ACIS-S/HEG in magenta and ACIS-S/MEG in purple.

european space agency
agence spatiale europ enne

Issue/Rev.:   6.0
Date: 23 December 2010

XMM Science Operations Team

Page: 36

C   Comparison of spectral response to lines

The scope of this section is to present the spectral response of the high resolution grating instruments at energies of various line triplets. For completeness, also the low resolution CCD instruments are included.

The different instrument responses were obtained by calculating the responses for specific observations applying the recent available public calibrations. Details are provided in Tab. 12.

The line triplets are faked with Gaussian model using the `fakeit`–command of XSPEC (version: 12.5.0ac) assuming 30 ksec of exposure time and using the line ratios for r:i:f of 5:1:3. In cases when two inter-combination line energies are used the intensity is equally split to both lines. All line energies are taken from the ATOMDB database and are listed in Tab. 13. The Gaussian line widths are fixed to 0.1 eV and the normalisation of the resonance line is fixed to photons cm^{-2} s^{-1}.

Fig. 32 provides and overview on the main line doublets and triplets of carbon, nitrogen, oxygen, neon, magnesium, silicon and sulphur. This overview is presented in energy space, whereas the individual triplets in Figs. 33-34 are presented in wavelength space.

The colours used are EPIC-pn in black, combined EPIC-MOS in green, combined XIS0+3 in purple, XIS1 in magenta, RGS1 in red, RGS2 in orange, ACIS-S LEG in cyan, ACIS-S MEG in azure, ACIS-S HEG in dark blue.

Table 12: Calibration version and details of the responses used for the line triplet fakes.

Satellite	Instrument	Obs.ID	Details
XMM–Newton	SASv10.0 and CCFs as of 01.08.2010.		
	EPIC-pn	0411780501	PKS2155-304 at 28.04.2010, SW mode, medium filter.
	EPIC MOS1/2	0411780501	PKS2155-304 at 28.04.2010, SW mode, medium filter
	RGS1/2	0411780501	PKS2155-304 at 28.04.2010, Spectro+Q mode
Chandra	CIAOv4.2 and CALDB 4.2.2.		
	ACIS-LEG	11965	PKS2155-304 at 29.04.2010, first orders (+1/-1)
	ACIS-MEG	8375	3C 273 at 25.06.2007, first orders (+1/-1)
	ACIS-HEG	8375	3C 273 at 25.06.2007, first orders (+1/-1)
Suzaku	HEASOFT 6.9, Suzaku software version 16.0, CALDB XIS 20100123		
	XIS0/3	105001010	PKS2155-304 at 28.04.2010, mode 3x3 + 5x5
	XIS1	105001010	PKS2155-304 at 28.04.2010, mode 3x3 + 5x5

Table 13: Line triplets of various ions and the energies/wavelengths of the resonance (r), inter-combination (i) and forbidden (f) lines used for the fake of the line triplets. All line energies are taken from ATOMDB.

Ion	Energies [keV]				Wavelengths [Å]			
	r	i		f	r	i		f
CV	0.3079	0.3044		0.2990	40.2674	40.7302		41.4715
NVI	0.4307	0.4262		0.4198	28.7870	29.0843		29.5347
OVII	0.5740	0.5686		0.5611	21.6015	21.8036		22.0977
NeIX	0.9220	0.9148		0.9051	13.4473	13.5531		13.6990
MgXI	1.3522	1.3435	1.3431	1.3311	9.1687	9.2282	9.2312	9.3143
SiXIII	1.8650	1.8547	1.8538	1.8394	6.6479	6.6850	6.6882	6.7403
SXV	2.4606	2.4488	2.4471	2.4303	5.0387	5.0631	5.0665	5.1015
FeXXV	6.7004	6.6823	6.6676	6.6366	1.8504	1.8554	1.8595	1.8682

european space agency
agence spatiale europ enne

Issue/Rev.: 6.0

Date: 23 December 2010

XMM Science Operations Team

Page: 37

Various line doublets and triplets
CV,CVI,NVI,NVII,OVII,OVIII,NeIX,NeX,MgXI,MgXII,SiXIII,SiXIV,SXV
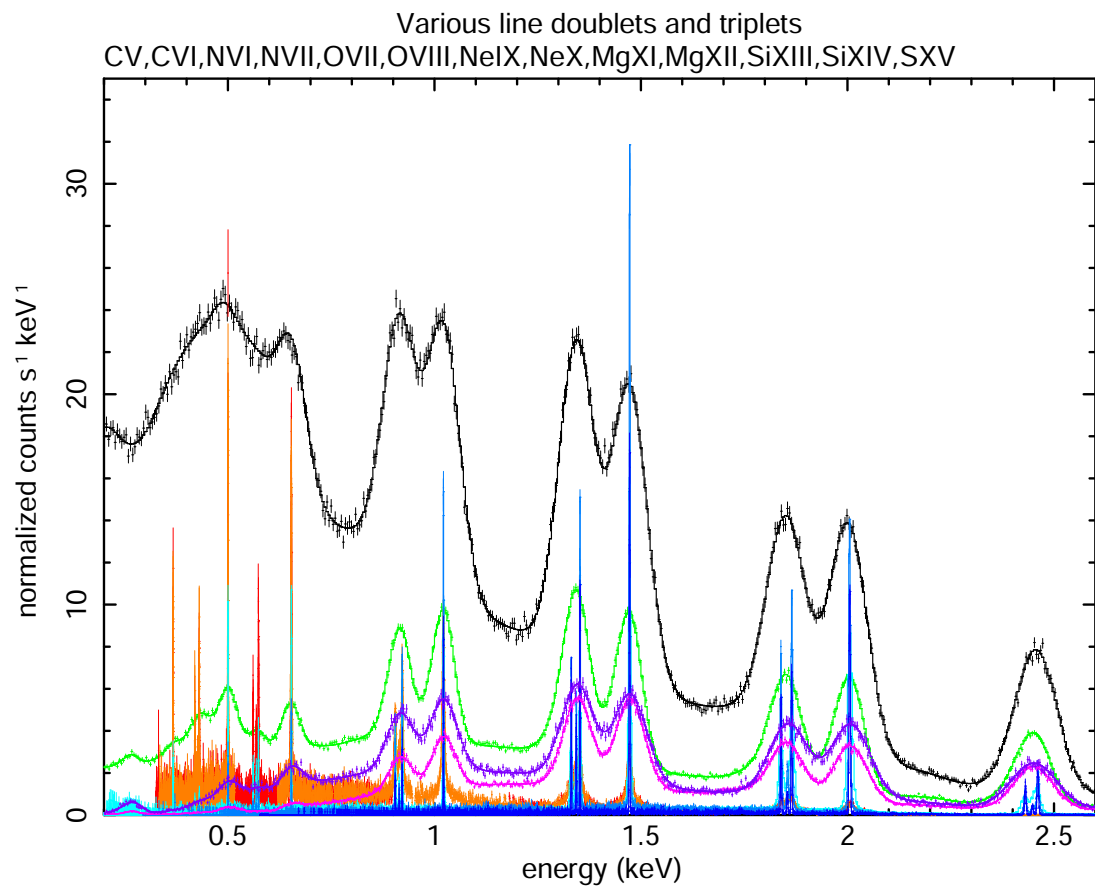

Figure 32: Overview of main H-like doublets and He-like triplets of various ions in energy space.
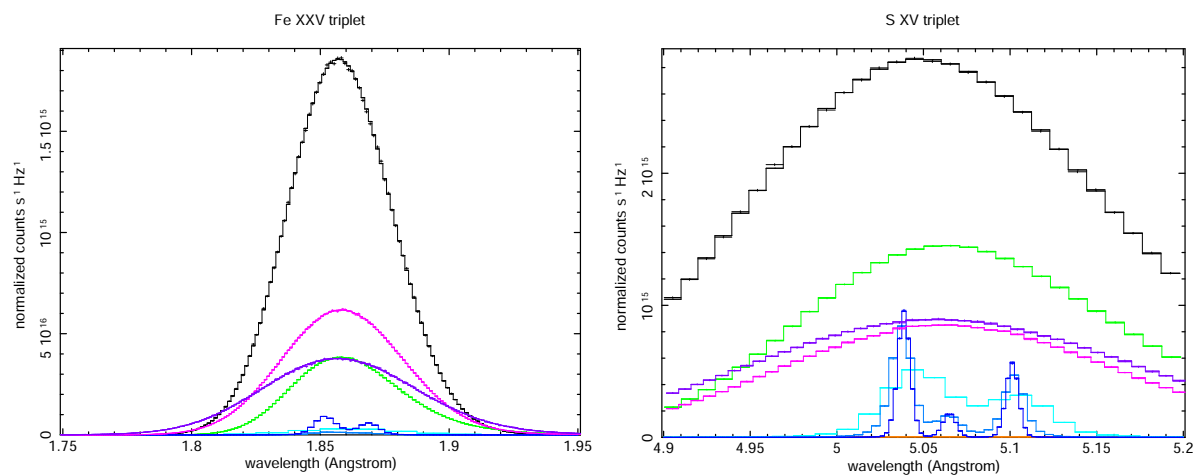

Figure 33: Line triplets of various ions. The colours used are EPIC-pn in black, combined EPIC-MOS in green, combined XIS0+3 in purple, XIS1 in magenta, RGS1 in red, RGS2 in orange, ACIS-S LEG in cyan, ACIS-S MEG in azure, ACIS-S HEG in dark blue.

european space agency
agence spatiale europ enne

Issue/Rev.: 6.0
Date: 23 December 2010

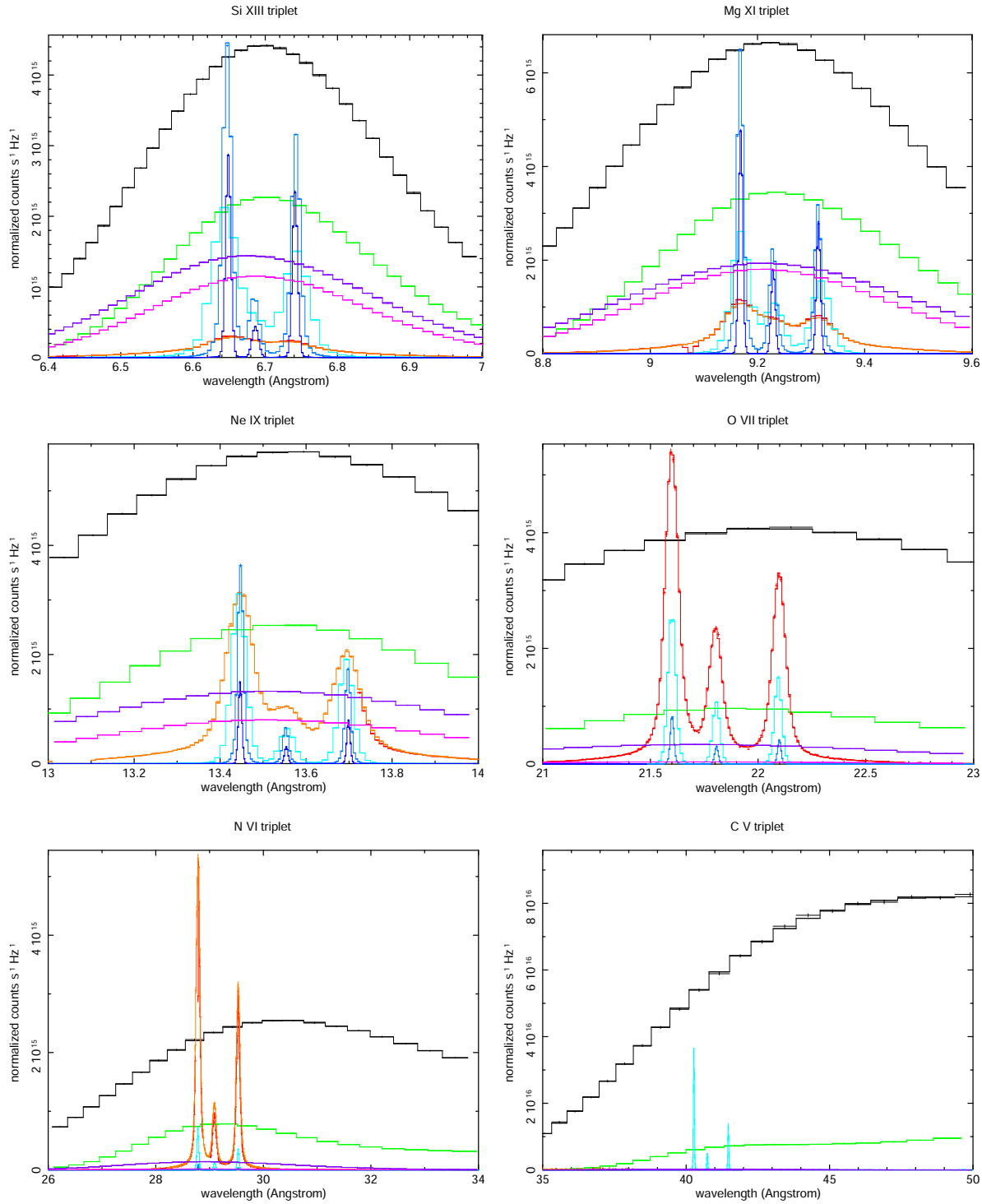**XMM Science Operations Team**

Page: 38

Figure 34: Line triplets of various ions. The colours used are EPIC-pn in black, combined EPIC-MOS in green, combined XIS0+3 in purple, XIS1 in magenta, RGS1 in red, RGS2 in orange, ACIS-S LEG in cyan, ACIS-S MEG in azure, ACIS-S HEG in dark blue.